



Delft University of Technology

Sandy coastlines under threat of erosion

Vousdoukas, Michalis I.; Ranasinghe, Roshanka; Mentaschi, Lorenzo; Plomaritis, Theocharis A.; Athanasiou, Panagiotis; Luijendijk, Arjen; Feyen, Luc

DOI

[10.1038/s41558-020-0697-0](https://doi.org/10.1038/s41558-020-0697-0)

Publication date

2020

Document Version

Accepted author manuscript

Published in

Nature Climate Change

Citation (APA)

Vousdoukas, M. I., Ranasinghe, R., Mentaschi, L., Plomaritis, T. A., Athanasiou, P., Luijendijk, A., & Feyen, L. (2020). Sandy coastlines under threat of erosion. *Nature Climate Change*, 10(3), 260-263.
<https://doi.org/10.1038/s41558-020-0697-0>

Important note

To cite this publication, please use the final published version (if applicable).

Please check the document version above.

Copyright

Other than for strictly personal use, it is not permitted to download, forward or distribute the text or part of it, without the consent of the author(s) and/or copyright holder(s), unless the work is under an open content license such as Creative Commons.

Takedown policy

Please contact us and provide details if you believe this document breaches copyrights.
We will remove access to the work immediately and investigate your claim.

1. Extended Data

Figure #	Figure title	Filename	Figure Legend
	One sentence only	This should be the name the file is saved as when it is uploaded to our system. Please include the file extension. i.e.: <i>Smith_ED_Fi_1.jpg</i>	If you are citing a reference for the first time in these legends, please include all new references in the Online Methods References section, and carry on the numbering from the main References section of the paper.
Extended Data Fig. 1	Geographical regions considered in the present analysis	Vousdoukas_E D_01.eps	Geographical regions considered in the present analysis, based on the IPCC SREX report and limited to those that contain ice-free sandy coastlines
Extended Data Fig. 2	Projected long term shoreline change due to SLR driven retreat (R) alone, by the year 2050 and 2100 under RCP4.5 and RCP8.5.	Vousdoukas_E D_02.eps	Projected long term shoreline change due to SLR driven retreat (R) alone, by the year 2050 (a,c) and 2100 (b,d) under RCP4.5 (a-b) and RCP8.5 (c-d). Values represent the median change and positive/negative values express accretion/erosion in m, relative to 2010. The global average median change is shown in the inset text for each case, along with the 5 th -95 th percentile range.
Extended Data Fig. 3	Projected long term shoreline change driven due to the ambient shoreline change rate (AC) alone, by the year 2050 and 2100.	Vousdoukas_E D_03.eps	Projected long term shoreline change driven due to the ambient shoreline change rate (AC) alone, by the year 2050 (a) and 2100 (b). Values represent the median change and positive/negative values express accretion/erosion in m, relative to 2010. The global average median change is shown in the inset text for each case, along with the 5 th -95 th percentile range.
Extended Data Fig. 4	Projected change in 100-year episodic beach erosion for the year 2050 and 2100 under RCP4.5 and	Vousdoukas_E D_04.eps	Projected change in 100-year episodic beach erosion for the year 2050 (a,c) and 2100 (b,d) under RCP4.5 (a-b) and RCP8.5 (c-d). Values represent the median change and positive/negative values express less/more erosion (m), relative to 2010. The global average median change is shown in

	RCP8.5.		the inset text for each case, along with the 5 th -95 th percentile range.
Extended Data Fig. 5	Projected median long term shoreline change under RCP4.5 by the year 2050 ($dx_{shore,LT}$), for the 26 IPCC SREX sub- regions and the worldwide average	Vousdoukas_E D_05.eps	Projected median long term shoreline change under RCP4.5 by the year 2050 ($dx_{shore,LT}$), for the 26 IPCC SREX sub- regions and the worldwide average (horizontal bar plot; positive/negative values express accretion/erosion in m). Shoreline change is considered to be the result of SLR retreat (R) and ambient shoreline change trends (AC). Pie plots show the relative contributions of R and AC to the projected median $dx_{shore,LT}$, with transparent patches expressing accretive trends. Vertical bar plots show the relative contributions of R and AC, as well as that of RCPs, to the total uncertainty in projected median $dx_{shore,LT}$.
Extended Data Fig. 6	Projected median long term shoreline change under RCP8.5 by the year 2050 ($dx_{shore,LT}$), for the 26 IPCC SREX sub- regions and the worldwide average	Vousdoukas_E D_06.eps	Projected median long term shoreline change under RCP8.5 by the year 2050 ($dx_{shore,LT}$), for the 26 IPCC SREX sub- regions and the worldwide average (horizontal bar plot; positive/negative values express accretion/erosion in m). Shoreline change is considered to be the result of SLR retreat (R) and ambient shoreline change trends (AC). Pie plots show the relative contributions of R and AC to the projected median $dx_{shore,LT}$, with transparent patches expressing accretive trends. Vertical bar plots show the relative contributions of R and AC, as well as that of RCPs, to the total uncertainty in projected median $dx_{shore,LT}$.
Extended Data Fig. 7	Projected median long term shoreline change under RCP4.5 by the year 2100 ($dx_{shore,LT}$), for the 26 IPCC SREX sub- regions and the worldwide average	Vousdoukas_E D_07.eps	Projected median long term shoreline change under RCP4.5 by the year 2100 ($dx_{shore,LT}$), for the 26 IPCC SREX sub- regions and the worldwide average (horizontal bar plot; positive/negative values express accretion/erosion in m). Shoreline change is considered to be the result of SLR retreat (R) and ambient shoreline change trends (AC). Pie plots show the relative contributions of R and AC to the projected

			median $dx_{shore,LT}$, with transparent patches expressing accretive trends. Vertical bar plots show the relative contributions of R and AC, as well as that of RCPs, to the total uncertainty in projected median $dx_{shore,LT}$.
Extended Data Fig. 8	Percentage length of sandy beach shoreline that is projected to retreat by more than 50, 100 and 200 m per IPCC SREX sub-region	Vousdoukas_E D_08.eps	Bar plots showing, per IPCC SREX sub-region, the percentage length of sandy beach shoreline that is projected to retreat by more than 50 (blue), 100 (yellow) and 200 m (red), by 2050 (a,c) and 2100 (b,d), under RCP4.5 (a-b) and RCP8.5 (c-d) relative to 2010. Transparent color patches indicate the 5 th -95 th quantile range and solid rectangles show the median value. For the region abbreviations, please see Extended Data Fig. 1.
Extended Data Fig. 9	Length of sandy beach shoreline that is projected to retreat by more than 50, 100 and 200 m per IPCC SREX sub-region	Vousdoukas_E D_09.eps	Bar plots showing, per IPCC SREX sub-region, the length (in km) of sandy beach shoreline that is projected to retreat by more than 50 (blue), 100 (yellow) and 200 m (red), by 2050 (a,c) and 2100 (b,d), under RCP4.5 (a-b) and RCP8.5 (c-d) relative to 2010. Transparent color patches indicate the 5 th -95 th quantile range and solid rectangles show the median value. For the region abbreviations, please see Supplementary Figs. S2 and S5
Extended Data Fig. 10	Per country length of sandy beach shoreline that is projected to retreat by more than 100 m	Vousdoukas_E D_10.eps	Per country length of sandy beach coastline which is projected to retreat by more than 100 m by 2050 (a,c) and 2100 (b,d), under RCP4.5 (a-b) and RCP8.5 (c-d). Values are based on the median long term shoreline change, relative to 2010.

3 **2. Supplementary Information:**

4 **A. Flat Files**

5

Item	Present?	Filename	A brief, numerical description of file contents.
		This should be the	

		name the file is saved as when it is uploaded to our system, and should include the file extension. The extension must be .pdf	i.e.: <i>Supplementary Figures 1-4, Supplementary Discussion, and Supplementary Tables 1-4.</i>
Supplementary Information	Yes	Vousdoukas_NLetter_SI.pdf	<i>Supplementary Figure 1, Supplementary Tables 1-4.</i>
Reporting Summary	Choose an item.		

6

7

8 B. Additional Supplementary Files

9

Type	Number	Filename	Legend or Descriptive Caption
Choose an item.	If there are multiple files of the same type this should be the numerical indicator. i.e. "1" for Video 1, "2" for Video 2, etc.	This should be the name the file is saved as when it is uploaded to our system, and should include the file extension. i.e.: <i>Smith_Supplementary_Video_1.mov</i>	Describe the contents of the file
Choose an item.			

10

11

12 3. Source Data

13

Parent Figure or Table	Filename	Data description
	This should be the name the file is saved as when it is uploaded to	e.g.: Unprocessed Western Blots and/or gels,

	our system, and should include the file extension. i.e.: <i>Smith_SourceData_Fig1.xls</i> , or <i>Smith_Unmodified_Gels_Fig1.pdf</i>	Statistical Source Data, etc.
Source Data Fig. 1		
Source Data Fig. 2		
Source Data Fig. 3		
Source Data Fig. 4		
Source Data Fig. 5		
Source Data Fig. 6		
Source Data Fig. 7		
Source Data Fig. 8		
Source Data Extended Data Fig. 1		
Source Data Extended Data Fig. 2		
Source Data Extended Data Fig. 3		
Source Data Extended Data Fig. 4		
Source Data Extended Data Fig. 5		

Source Data Extended Data Fig. 6		
Source Data Extended Data Fig. 7		
Source Data Extended Data Fig. 8		
Source Data Extended Data Fig. 9		
Source Data Extended Data Fig. 10		

14

15 Sandy coastlines under threat of erosion

16

17 Michalis I. Voudoukas^{1*}, Roshanka Ranasinghe^{2,3,4}, Lorenzo Mentaschi¹, Theocharis A. Plomaritis^{5,6},
18 Panagiotis Athanasiou^{3,4}, Arjen Luijendijk^{4,7}, Luc Feyen¹

19 ¹European Commission, Joint Research Centre (JRC), Email: Michail.VOUSDOUKAS@ec.europa.eu; Tel:
20 +39 033278-6499; Fax: +39 033278-665

21 ²Department of Water Science and Engineering, IHE Delft Institute for Water Education, PO Box 3015,
22 2610 DA Delft, the Netherlands

23 ³Water Engineering and Management, Faculty of Engineering Technology, University of Twente, PO, Box
24 217, 7500 AE Enschede, the Netherlands

25 ⁴Harbour, Coastal and Offshore Engineering, Deltas, PO Box 177, 2600 MH Delft, the Netherlands

26 ⁵University of Cadiz, Dpt. Applied Physics, CASEM, University of Cadiz, 11510 Puerto Real, Cádiz, Spain

27 ⁶CIMA, University of Algarve, Campus de Gambelas, 8005-139, Faro, Portugal

28 ⁷Faculty of Civil Engineering and Geosciences, Department of Hydraulic Engineering, Delft University of
29 Technology, P.O. Box 5048, 2600 GA Delft, The Netherlands

30

31 *Corresponding author address:

32 Dr Michalis Voudoukas

33 European Commission, Joint European Research Centre (JRC), Via Enrico Fermi 2749, I-21027, Ispra,

34 Italy. Email: Michail.VOUSDOUKAS@ec.europa.eu; Tel: +39 033278-6499; Fax: +39 033278-665

35

36 Sandy beaches occupy more than one third of the global coastline¹ and have high socio-
37 economic value related to recreation, tourism, and ecosystem services². Beaches are the interface
38 between land and ocean, providing coastal protection from marine storms and cyclones³. However
39 the presence of sandy beaches cannot be taken for granted, as they are under constant change, driven
40 by meteorological^{4,5}, geological⁶, and anthropogenic factors^{1,7}. A substantial proportion of the world's
41 sandy coastline is already eroding^{1,7}, a situation that could be exacerbated by climate change^{8,9}. Here,
42 we show that with, climate mitigation, ambient trends in shoreline dynamics, combined with coastal
43 recession driven by sea level rise could result in the near extinction of almost half of the world's sandy
44 beaches by the end of the century. Moderate greenhouse gas emission mitigation could prevent 40%
45 of shoreline retreat. Projected shoreline dynamics are dominated by sea level rise for the majority of
46 sandy beaches, but in certain regions this is overshadowed by ambient shoreline changes. In West and
47 East Asia, long-term accretion up to 200-300 m is projected. A significant proportion of the threatened
48 sandy shorelines are in densely populated areas, underlining the need for the design and
49 implementation of effective adaptive measures.

50

51 The coastal zone is among the most developed areas worldwide, containing an abundance of
52 developments, critical infrastructure¹⁰, and ecosystems^{2,3}. As a result, population density tends to be
53 higher near the coast¹¹, and most projections indicate that current trends of coastward migration,
54 urbanization and population growth will continue^{12,13}. Of the different beach typologies found
55 worldwide sandy beaches are the most heavily utilized¹⁴ and are among the most geomorphologically
56 complex, with the shoreline, i.e. the mean water line along the coast, changing constantly under forcing-
57 response interactions between natural and anthropogenic factors⁷.

58 The global mean sea level has been increasing at an accelerated rate during the past 25 years¹⁵ and will
59 continue to do so in view of climate change^{16,17}. While shoreline change can be the combined result of a
60 wide range of potentially erosive or accretive factors⁸, there is a clear cause and effect relation between
61 increasing sea levels and shoreline retreat¹⁸, pointing to increased coastal erosion issues^{9,19}. Climate
62 change will also affect waves and storm surges^{20,21}, which are important drivers of coastal
63 morphology^{4,5,22}, and therefore considering the dynamics of extreme weather patterns is also important
64 in assessing potential climate change impacts beyond that of SLR alone.

65 Here we present a comprehensive global analysis of sandy shoreline dynamics during the 21st century.
66 Our probabilistic projections explicitly take into account estimates of future SLR, spatial variations of
67 coastal morphology, ambient shoreline change trends, and future changes in meteorological drivers (e.g.
68 storm surge and waves). We first evaluate long term shoreline change dx_{shore_LT} , which is the result of
69 two components: the ambient shoreline change (AC) driven by geological, anthropogenic and other
70 physical factors⁷ and the shoreline retreat due to SLR (R) (Supplementary Fig. S1). We obtained AC by
71 extrapolating observed historical trends⁷ within a probabilistic framework (see Methods). We computed
72 R by using a modified Bruun rule¹⁸ together with a new global dataset of active beach slopes²³. In
73 addition to the long term shoreline dynamics we also project how maximum erosion from coastal
74 storms may change in view of climate change. Shoreline change projections are discussed for the years
75 2050 and 2100 under RCP 4.5 and 8.5, relative to the baseline year 2010.

76 Our analysis shows an overall erosive trend of sandy beaches that increases in time and with the
77 intensity of greenhouse gas emissions (Figure 1). Assuming that there are no physical limits in potential
78 retreat, by mid-century we project a very likely (5-95th percentile) global average long term shoreline
79 change $dx_{shore,LT}$ ranging from -2.2 to -79.2 m and -0.8 to -99.2 m,, under RCP4.5 and RCP8.5, respectively
80 (negative values express erosion; Supplementary Table S1). By the end of the century the erosive trend
81 becomes even more dominant and we project a very likely range from -21.7 to -171.1 m and -42.2 to -
82 246.9 m under RCP4.5 and RCP8.5, respectively (Figure 2 Supplementary Table S1). Moderate
83 greenhouse gas emission mitigation could thus prevent 22% of the projected shoreline retreat by 2050
84 and 40% by the end of the century (Supplementary Table S1). This corresponds to a global average of
85 around 42 m of preserved sandy beach width by the end of the century.

86 The global erosive trend masks high spatial variability, with erosive and accretive tendencies
87 interchanging across regions and along nearby coastal segments (Figure 1). Whereas local trends can
88 exceed several meters per year, eight IPCC sub-regions show median retreats exceeding 100 m under

89 both RCPs by the end of the century (Supplementary Table S1; see Figure 2 for a definition of the
90 regions): East North America, Amazon, Southeastern South America, Central Europe, South and West
91 Asia, North Australia, and the Caribbean SIDS. By 2100, $dx_{shore,LT}$ exceeds 150 m under RCP8.5 in all the
92 above regions, while under the same scenario median retreats larger than 300 m are projected for
93 South Asia and the Caribbean SIDS. Long term accretion is projected along sandy coastlines of East Asia
94 under both RCPs by 2050 and only under RCP4.5 by the end of the century.

95 SLR driven retreat R is responsible for 71% and 75% of the global median shoreline change in 2050 under
96 RCP4.5 and RCP8.5, respectively (Extended data Figs 5-6); and for 86% and 77% by the end of the
97 century (Figure 2 and Extended Data Fig. 7). Ambient shoreline changes dominate only in certain
98 regions, in particular in South and West Asia, West Indian Ocean, Southeastern South America, and the
99 Caribbean SIDS regions. The contributions of the SLR retreat and ambient change to the overall
100 uncertainty under RCP4.5 and by mid-century are relatively balanced (Extended Data Fig. 5), while AC
101 contributes to 41% more uncertainty globally, by the end of the century (Extended Data Fig. 7). Under
102 RCP8.5 uncertainty related to SLR retreat dominates that of AC, by 44% and 30%, by the years 2050 and
103 2100, respectively (Extended Data Fig. 7 and Figure 2). Regionally, ambient change uncertainty is higher
104 in North Australia South Asia.

105 The above estimates do not include the episodic, storm-driven shoreline retreat S , presently projected
106 using the convolution erosion model of Kriebel and Dean²⁴ (see Methods). Here we discuss the 100-year
107 event S which for the year 2050 is equivalent to circa 23% of the global average projected long term
108 shoreline change $dx_{shore,LT}$ (Supplementary Tables S1-4). By the end of the 21st century, the relative
109 importance of the 100-year S compared to $dx_{shore,LT}$ decreases to 9% and 7% under RCP4.5 and 8.5,
110 respectively, as long term changes gather pace. Storm erosion is typically followed by beach recovery²⁵,
111 but some events may leave a footprint that takes decades to recover, if at all^{4,26}, while the additional
112 shoreline retreat renders the backshore more vulnerable to episodic coastal flooding and its
113 consequences. Despite previous studies projecting changes in wave intensity and direction
114 worldwide^{21,27,28}, our projections show that overall climate change will not have a strong effect on
115 episodic storm driven erosion. As a result, ambient and SLR driven change appear to shadow the effect
116 of changes in storm-driven erosion, even though at certain locations ΔS values can reach ± 20 m by the
117 end of the century; e.g. increase in 100-year erosion potential along the South East UK, West coast of
118 Germany, North Queensland (Australia), and Acapulco (Mexico) (Extended Data Fig. 4).

119 The projected shoreline changes will substantially impact on the shape of the world's coastline. Many
120 coastal systems have lost already their natural capacity to accommodate or recover from erosion, as the
121 backshore is heavily occupied by human settlements²⁹, while dams and human development have
122 depleted terrestrial sediment supply which would naturally replenish the shore with new material^{30,31}.
123 Most of the remaining regions with an extensive presence of a natural coastline, are found in Africa and
124 Asia, which are also the regions projected to experience the highest coastal population and urbanization
125 growth in the decades to come^{12,13}. There is yet no global dataset on sandy beach width allowing to
126 accurately estimate the potential loss of sandy beaches around the world. Therefore, to quantify the
127 potential impact of our projections, we consider beaches that are projected to experience a shoreline
128 retreat >100 m as seriously threatened by coastal erosion. The chosen 100 m threshold is rather
129 conservative, since most sandy beaches have widths below 50 m, especially near human settlements,
130 small islands and micro-tidal areas (e.g. Caribbean, Mediterranean).

131 We find that 10.6%-12.2% (28,260-32,456 km) of the world's sandy beaches could face severe erosion
132 by 2050 and 37.2%-50.9% (99,996-135,279 km) by the end of the century (Extended Data Fig. 8). Thirty
133 one percent (31%) of the world's sandy beaches are in low elevation coastal zones (LECZ) with
134 population density exceeding 500 people per km², and our projections show that approximately one
135 third of these LECZ sandy coasts will be seriously threatened by erosion by the year 2050. This estimate
136 reaches 51% and 62% by the end of the century, under RCP4.5 and RCP8.5, respectively.

137 Several countries could face extensive erosion by the end of the 21st century (along >80% of their sandy
138 coastline under both RCPs; Figure 3) including Democratic Republic of the Congo, Gambia, Jersey,
139 Suriname, Comoros, Palau, Benin, Guinea-Bissau, Mayotte, Iraq, Pakistan, Guinea and El Salvador. Apart
140 from the consequent higher vulnerability to coastal hazards, several of these countries are likely to
141 experience substantial socioeconomic implications as their economies are fragile and, tourism-
142 dependent with sandy coastlines constituting their major tourist attraction. When the total length of
143 sandy beaches projected to be lost by 2100 is considered (as opposed to the %), Australia emerges as the
144 potentially most affected country, with at least 12,324 km of sandy beach coastline threatened by
145 erosion (15,439 under RCP8.5; Extended Data Fig. 9), circa 40% of the country's total sandy coastline. By
146 the same impact metric, Canada ranks second (9,577 and 16,651 km 15,439 under RCP4.5 and RCP8.5,
147 respectively), followed by Chile (5,471 and 7,050 km), Mexico (4,119 and 5,105 km) China (4,084 and
148 5,185 km), USA (3,908 and 5,553 km), Argentina (3,668 and 4,413 km) and Iran (3,654 and 3,870 km).

149 Past experience has shown that effective site-specific coastal planning can mitigate beach erosion,
150 eventually resulting in a stable coastline; with the most prominent example being the Dutch coast³². A
151 positive message from the present analysis is that while SLR will drive shoreline retreat almost
152 everywhere, many locations show ambient erosive trends related to human interventions⁷, which in
153 theory could be avoided by more sustainable coastal zone and catchment management practices. At the
154 same time, the range of projected SLR implies unprecedented pressure to our coasts which requires the
155 development and implementation of informed and effective adaptive measures.

156 CORRESPONDENCE

157 Correspondence and requests for materials should be addressed to M.I.V.

158 References

- 159 1 Luijendijk, A. *et al.* The State of the World's Beaches. *Scientific Reports* **8**, 6641, doi:10.1038/s41598-018-24630-6 (2018).
- 160 2 Barbier, E. B. *et al.* The value of estuarine and coastal ecosystem services. *Ecological Monographs* **81**, 169-193, doi:10.1890/10-1510.1 (2011).
- 161 3 Temmerman, S. *et al.* Ecosystem-based coastal defence in the face of global change. *Nature* **504**, 79, doi:10.1038/nature12859 (2013).
- 162 4 Masselink, G. *et al.* Extreme wave activity during 2013/2014 winter and morphological impacts along the Atlantic coast of Europe. *Geophys. Res. Lett.* **43**, 2135-2143, doi:10.1002/2015GL067492 (2016).
- 163 5 Barnard, P. L. *et al.* Coastal vulnerability across the Pacific dominated by El Nino/Southern Oscillation. *Nat. Geosci.* **8**, 801-807, doi:10.1038/ngeo2539 (2015).
- 164 6 Cooper, J. A. G., Green, A. N. & Loureiro, C. Geological constraints on mesoscale coastal barrier behaviour. *Global Planet. Change* **168**, 15-34, doi:<https://doi.org/10.1016/j.gloplacha.2018.06.006> (2018).
- 165 7 Mentaschi, L., Vousdoukas, M. I., Pekel, J.-F., Voukouvalas, E. & Feyen, L. Global long-term observations of coastal erosion and accretion. *Scientific Reports* **8**, 12876, doi:10.1038/s41598-018-30904-w (2018).
- 166 8 Ranasinghe, R. Assessing climate change impacts on open sandy coasts: A review. *Earth-Science Reviews* **160**, 320-332, doi:<https://doi.org/10.1016/j.earscirev.2016.07.011> (2016).
- 167 9 Hinkel, J. *et al.* A global analysis of erosion of sandy beaches and sea-level rise: An application of DIVA. *Global Planet. Change* **111**, 150-158, doi:<https://doi.org/10.1016/j.gloplacha.2013.09.002> (2013).
- 168 10 Koks, E. E. *et al.* A global multi-hazard risk analysis of road and railway infrastructure assets. *Nature Communications* **10**, 2677, doi:10.1038/s41467-019-10442-3 (2019).
- 169 11 McGranahan, G., Balk, D. & Anderson, B. The rising tide: assessing the risks of climate change and human settlements in low elevation coastal zones. *Environment and Urbanization* **19**, 17-37, doi:10.1177/0956247807076960 (2007).
- 170 12 Neumann, B., Vafeidis, A. T., Zimmermann, J. & Nicholls, R. J. Future Coastal Population Growth and Exposure to Sea-Level Rise and Coastal Flooding - A Global Assessment. *PLOS ONE* **10**, e0118571, doi:10.1371/journal.pone.0118571 (2015).

- 189 13 Jones, B. & O'Neill, B. C. Spatially explicit global population scenarios consistent with the Shared
190 Socioeconomic Pathways. *Environmental Research Letters* **11**, doi:10.1088/1748-
191 9326/11/8/084003 (2016).
- 192 14 Davenport, J. & Davenport, J. L. The impact of tourism and personal leisure transport on coastal
193 environments: A review. *Estuar. Coast. Shelf Sci.* **67**, 280-292,
194 doi:<https://doi.org/10.1016/j.ecss.2005.11.026> (2006).
- 195 15 Nerem, R. S. *et al.* Climate-change–driven accelerated sea-level rise detected in the altimeter
196 era. *Proceedings of the National Academy of Sciences* **115**, 2022-2025,
197 doi:10.1073/pnas.1717312115 (2018).
- 198 16 Bamber, J. L., Oppenheimer, M., Kopp, R. E., Aspinall, W. P. & Cooke, R. M. Ice sheet
199 contributions to future sea-level rise from structured expert judgment. *Proceedings of the
200 National Academy of Sciences*, 201817205, doi:10.1073/pnas.1817205116 (2019).
- 201 17 Jevrejeva, S., Jackson, L. P., Riva, R. E. M., Grinsted, A. & Moore, J. C. Coastal sea level rise with
202 warming above 2 °C. *Proceedings of the National Academy of Sciences* **113**, 13342-13347,
203 doi:10.1073/pnas.1605312113 (2016).
- 204 18 Bruun, P. Sea level rise as a cause of shore erosion. *Journal of Waterway, Harbors Division. ASCE*
205 **88**, 117 (1962).
- 206 19 Anthony, E. J. *et al.* Linking rapid erosion of the Mekong River delta to human activities.
207 *Scientific Reports* **5**, 14745, doi:10.1038/srep14745 (2015).
- 208 20 Vousdoukas, M. I. *et al.* Global probabilistic projections of extreme sea levels show
209 intensification of coastal flood hazard. *Nature Communications* **9**, 2360, doi:10.1038/s41467-
210 018-04692-w (2018).
- 211 21 Hemer, M. A., Fan, Y., Mori, N., Semedo, A. & Wang, X. L. Projected changes in wave climate
212 from a multi-model ensemble. *Nature Clim. Change* **3**, 471-476, doi:10.1038/nclimate1791
213 (2013).
- 214 22 Slott, J. M., Murray, A. B., Ashton, A. D. & Crowley, T. J. Coastline responses to changing storm
215 patterns. *Geophys. Res. Lett.* **33**, doi:10.1029/2006GL027445 (2006).
- 216 23 Athanasiou, P. *et al.* A global dataset of coastslopes for coastal recession assessments. *Earth
217 System Science Data Discussions* **11**, 1515–1529, doi:<https://doi.org/10.5194/essd-11-1515-2019> (2019).
- 219 24 Kriebel, D. L. & Dean, R. G. Convolution method for time dependent beach profile response.
220 *Journal of Waterway, Port, Coastal and Ocean Engineering* **119**, 204-226 (1993).
- 221 25 Vousdoukas, M. I. Erosion/accretion patterns and multiple beach cusp systems on a meso-tidal,
222 steeply-sloping beach. *Geomorphology* **141**, 34-46, doi:10.1016/j.geomorph.2011.12.003 (2012).
- 223 26 Anderson, T. R., Frazer, L. N. & Fletcher, C. H. Transient and persistent shoreline change from a
224 storm. *Geophys. Res. Lett.* **37**, doi:10.1029/2009gl042252 (2010).
- 225 27 Erikson, L. H., Hegermiller, C. A., Barnard, P. L., Ruggiero, P. & van Ormondt, M. Projected wave
226 conditions in the Eastern North Pacific under the influence of two CMIP5 climate scenarios.
227 *Ocean Modelling* **96**, 171-185, doi:<https://doi.org/10.1016/j.ocemod.2015.07.004> (2015).
- 228 28 Mentaschi, L., Vousdoukas, M. I., Voukouvalas, E., Dosio, A. & Feyen, L. Global changes of
229 extreme coastal wave energy fluxes triggered by intensified teleconnection patterns. *Geophys.
230 Res. Lett.* **44**, 2416-2426, doi:10.1002/2016GL072488 (2017).
- 231 29 Small, C. & Nicholls, R. J. A Global Analysis of Human Settlement in Coastal Zones. *J. Coast. Res.*
232 **19**, 584-599 (2003).
- 233 30 Milliman, J. D. Blessed dams or damned dams? *Nature* **386**, 325-327, doi:10.1038/386325a0
234 (1997).

- 235 31 Ranasinghe, R., Wu, C. S., Conallin, J., Duong, T. M. & Anthony, E. J. Disentangling the relative
236 impacts of climate change and human activities on fluvial sediment supply to the coast by the
237 world's large rivers: Pearl River Basin, China. . *Scientific Reports* (accepted).
- 238 32 Brière, C., Janssen, S. K. H., Oost, A. P., Taal, M. & Tonnon, P. K. Usability of the climate-resilient
239 nature-based sand motor pilot, The Netherlands. *J. Coast. Conserv.* **22**, 491-502,
240 doi:10.1007/s11852-017-0527-3 (2018).
- 241

242 **Figure captions**

243 *Figure 1. Projected long term shoreline change. By the year 2050 (a,c) and 2100 (b,d) under RCP4.5 (a-b) and RCP8.5 (c-d).*
244 *Values represent the median change and positive/negative values respectively express accretion/erosion in m, relative to 2010.*
245 *The global average median change is shown in the inset text for each case, along with the 5th-95th percentile range.*

246

247 *Figure 2. Projected median long term shoreline change under RCP8.5 by the year 2100 ($dx_{shore,LT}$), for the 26 IPCC SREX sub-*
248 *regions and the worldwide average. For the horizontal bar plot on right; positive/negative values express accretion/erosion in m;*
249 *black error bars indicate the 5th-95th quantile range. Shoreline change is considered to be the result of SLR retreat (R) and*
250 *ambient shoreline change trends (AC). Pie plots show the relative contributions of R and AC to the projected median $dx_{shore,LT}$,*
251 *with transparent slices expressing accreptive trends. Vertical bar plots show the ratio between the uncertainty of R and AC (5th-*
252 *95th quantile range), to the total uncertainty in projected median $dx_{shore,LT}$.*

253

254 *Figure 3. Per country percentages of the sandy coastline length which is projected to retreat by more than 100 m. By 2050 (a,c)*
255 *and 2100 (b,d), under RCP4.5 (a-b) and RCP8.5 (c-d). Values are based on the median long term shoreline change, relative to*
256 *2010.*

257

258 [1 Methods](#)

259 [1.1 General concepts](#)

260 In this study we project shoreline dynamics throughout this century along the world's sandy coastlines
261 under two Representative Concentration Pathways (RCPs): RCP4.5 and RCP8.5. RCP4.5 may be viewed
262 as a *moderate-emission-mitigation-policy scenario* and RCP8.5 as a *high-emissions scenario*³³. The study
263 focusses on the evolution of three components of sandy beach shoreline dynamics (Supplementary Fig.
264 S1):

- 265 - AC: Ambient shoreline dynamics driven by long-term hydrodynamic, geological and anthropic
266 factors.
- 267 - R: Shoreline retreat due to coastal morphological adjustments to Sea Level Rise (SLR).
- 268 - S: Episodic erosion during extreme storms.

269 The first two components represent longer term shoreline changes and are quantified here as:

270
$$dx_{shore,LT} = AC + R \quad 1$$

271 AC expresses long-term ambient shoreline dynamics that can be driven by a wide range of natural
272 and/or anthropogenic processes, excluding the effect of SLR (R) and that of episodic erosion during
273 extreme events (S; see following paragraph). In most cases AC is related to human interventions that
274 alter the sediment budget and/or transport processes of coastal systems⁷, but it also includes natural
275 transitions due to a variety of reasons, such as weather patterns^{4,34-36}, persistent longshore transport
276 variations³⁷, or geological control^{38,39}. R in Eq. 1 represents SLR-driven shoreline retreat, the magnitude
277 of which depends on the transfer of sediment from the sub-aerial to the submerged part of the active
278 beach profile, in order to adjust to rising Mean Sea Levels (MSLs).

279 The third component S represents episodic erosion from intense waves and storm surges during
280 extreme weather events. Episodic erosion is usually followed by a recovery process⁴⁰⁻⁴². It is assumed
281 here that the irreversible net effect of episodic erosion and post-storm recovery constitutes part of the
282 ambient shoreline evolution expressed by AC. S is therefore limited to the reversible episodic shoreline
283 retreat during storm events relative to its long term position expressed by $dx_{shore,LT}$. Potential variations
284 in storminess with global warming will induce changes in S compared to present day conditions.

285 At any point in time, the maximum shoreline retreat $dx_{shore,max}$ during an extreme coastal event due to
286 the combined effects of long-term and episodic erosion is then defined as

287
$$dx_{shore,max} = AC + R + S \quad 2$$

288 Each of these components are discussed in more detail below.

289 This study focuses on ice-free sandy beaches, which constitute the most common and dynamic beach
290 type globally, covering more than 30% of the ice-free coastline in the world^{1,43}. While in reality shoreline
291 retreat can be limited by the presence of natural or anthropogenic barriers, spatial data on such
292 features is not available globally at the resolution needed for the present study. Adaptive measures
293 against beach erosion could have a similar effect, but are difficult to predict and merit a separate study.
294 Therefore, we do not invoke any physical limits to the extent of potential shoreline retreat.

295 [1.2 Ambient shoreline dynamics](#)

296 Several parts of the global coastline undergo long-term ambient changes as a result of various
297 hydrodynamic, geological and anthropic factors. Historical shoreline trends were estimated by
298 Mentaschi et al.⁷ from the high-resolution Global Surface Water (GSW) database⁴⁴. It provides spatio-
299 temporal dynamics of surface water presence globally at 30 m resolution from 1984 to 2015, obtained
300 by the automated analysis of over 3 million Landsat satellite images. This GSW dataset was processed
301 for changes in water presence in coastal areas to produce time series of cross-shore shoreline position⁷.
302 The pixel-wise information of GSW was translated into cross-shore shoreline dynamics using a set of
303 over 2,000,000 shore-normal transects. The transects were defined every 250 m along a global coastline
304 obtained from OpenStreetMap⁴⁵ and were sufficiently long to accommodate the shoreline displacement
305 during the study period. Each transect defines a 200 m alongshore-wide coastal section, along which
306 surface water transitions were considered in order to extract time-series of shoreline displacement
307 along each shore normal transect.

308 We consider as a proxy for the shoreline change the cross-shore displacement of the seaward boundary
309 of the ‘permanent land layer’; i.e. the areas where water presence has never been detected throughout
310 the year. Over the 32-year period considered, the selected proxy can respond to tidal, storm surge,
311 wave and swash dynamics, as well as the inter-related dynamics of the beach face slope or nearshore
312 bathymetry. Among the different shoreline definitions proposed in literature⁴⁶, the present one was
313 chosen as it is more compatible with the type of analysis and the spatial and temporal resolution of the

314 satellite dataset⁴⁶. A detailed description of the procedure, the data, and also links to the final dataset
315 can be found in Pekel et al.⁴⁴, and Mentaschi et al.⁷.

316 For the purpose of determining AC in the present study, we consider shoreline dynamics data for a 32-
317 year period (1984-2015) from Mentaschi et al.⁷. We assume that this time series is representative for
318 present-day ambient shoreline changes and extrapolate the trend into the future using a probabilistic
319 approach. For each location, we consider the time series of all transects that are within 5 km distance
320 along the same coastline stretch. This acts as a spatial smoothing in order to filter out local trends and
321 reflects changes at km scale, which are more relevant in a global scale analysis. It further ensures that
322 each transect has sufficient data and compensates for gaps in the satellite measurements due to poor
323 quality or lack of data. The original dataset comes with confidence indicators and low-confidence
324 measurements are excluded from the analysis. Similarly, shoreline changes that exceed 5 km in a year
325 are also excluded as outliers.

326 The above analysis results in sets of annual shoreline displacements for each point, which are sampled
327 randomly to generate synthetic series of future shoreline position with an annual time step. The Monte
328 Carlo sampling results in one million realizations of future shoreline evolution, resulting in Probability
329 Density Functions (PDFs) of annual shoreline displacement during the present century in each transect.
330 The number of realizations was taken to ensure a stable PDF of the shoreline changes by the end the
331 century in all studied transects, i.e. when the mean and the standard deviation of the PDFs converged.
332 The realizations of future shoreline evolution assume that ambient change will follow historical trends
333 and express the uncertainty of the historical observations.

334 1.3 Shoreline retreat due to SLR

335 The estimation of the equilibrium shoreline retreat R of sandy coasts due to SLR is based on the Bruun
336 rule¹⁸. This approach builds on the concept that the beach morphology tends to adapt to the prevailing
337 wave climate and is given by:

$$338 R = \frac{1}{\tan\beta} SLR$$

3

339

340 where $\tan\beta$ is the active profile slope.

341 Projections of regional SLR up to the end of this century are available from a probabilistic, process-based
342 approach⁴⁷ that combines the major factors contributing to SLR: impact of self-attraction and loading of

343 the ocean upon itself due to the long term alteration of ocean density changes, globally averaged steric
344 sea-level change, dynamic sea-level change, surface mass balance of ice from glaciers and ice-caps,
345 surface mass balance and ice dynamics of Greenland and Antarctic ice sheet, land-water storage and
346 Glacial Isostatic Adjustment. Local smaller scale vertical land movements such as land subsidence due to
347 for example ground water pumping are not included in the SLR projections.

348 The $\tan\beta$ term in equation 3 expresses the slope of the active beach profile, which to date typically has
349 been assumed to be constant (in space) in large scale studies⁹. Here, we use a newly released global
350 dataset of active beach slopes²³. The dataset has been created combining the MERIT digital elevation
351 dataset⁴⁸ with the GEBCO bathymetry⁴⁹. Beach profiles are generated along each sandy beach transect
352 by combining the above bathymetric and topographic data. The offshore boundary of the active profile
353 is defined by the furthest location from the coast with a depth equal to the depth of closure d_c . The
354 latter is calculated using an adaptation of the original Hallermeier 1978⁵⁰ formula by Nicholls et al. 1998⁵¹
355 for applications on longer time scales, given by:

$$356 \quad d_c = 2.28H_{e,t} - 68.5 \left(\frac{H_{e,t}^2}{gT_{e,t}^2} \right)$$

4

357 where $H_{e,t}$ is the significant wave height that is exceeded only 12 hours per t years, $T_{e,t}$ is the associated
358 wave period, and g is the gravitational acceleration. In this case t is equivalent to the 1980-2100 period.

359 The landward active profile boundary varies among studies and has been defined as the crest of the
360 berm or dune, or the most offshore location with an elevation equal to the MSL. In the absence of
361 reliable estimates of the dune or berm height B , and following the original definition of the Bruun Rule¹⁸
362 and its application in several recent studies^{9,52,53}, here we take the MSL contour as the landward active
363 profile boundary. The cross-shore distance between these two points is considered as the length of the
364 active profile L_b , of which the slope is defined as $\tan\beta = \frac{d_c}{L_b}$.

365 Waves are simulated over the period 1980 to 2100 using the third generation spectral wave model
366 WAVEWATCH-III forced by atmospheric conditions from 6 CMIP5 GCMs^{28,54}. The model runs on a global
367 1.5° grid, combined with several nested finer sub-grids with resolution varying from 0.5° to 0.5° . The
368 model's skill to reproduce global wave fields was assessed by comparing time series from a reanalysis
369 covering 35 years between 1980 and 2014, forced by ERA-Interim wind data, against altimeter data
370 provided by 6 different satellites⁵⁵: ERS-2, ENVISAT, Jason 1 and 2, Cryosat 2 and SARAL-AltiKa. Point
371 measurements provided by buoys were used for additional validation. Detailed information on the
372 model set-up and validation can be found in the references provided^{28,54}.

373 Several recent studies in Australia⁴¹, Netherlands⁵⁶, Spain⁵⁷ and France⁵⁸ that compared coastline retreat
374 projections obtained via the physics based Probabilistic coastline recession (PCR) modelwith those
375 derived with the Bruun rule have indicated that the latter consistently provides higher-end estimates of
376 coastline retreat. Acknowledging that the extent of overestimation depends on site-specific factors, we
377 therefore include in our probabilistic framework a correction factor E , which varies randomly between
378 0.1 and 1.0 centered around a conservative median value 0.75. Thus, here we compute SLR driven
379 shoreline retreat using the equation:

380
$$R = E \cdot \frac{1}{\tan\beta} \cdot SLR$$

5

381 Finally, the active beach slope analysis detected that $\tan\theta$ values in some parts of the world can be as
382 mild as 1/800. According to the Bruun rule and the projected range of SLR, such mild sloping coastal
383 zones will experience shoreline retreats of several hundreds of meters. While not impossible, such
384 estimates could yield serious potential overestimations of real-world shoreline adjustment to SLR⁵⁹. We
385 therefore limit the minimum beach slope to 1/300, which is a realistic lower bound estimate for sandy
386 beaches.

387 As SLR retreat is estimated in a probabilistic manner through Monte Carlo simulations, the resulting
388 PDFs express the uncertainty from the SLR projections and the Bruun rule error expressed through the E
389 correction factor.

390 1.4 Storm-induced erosion

391 Episodic erosion during extreme storms is estimated using the convolution erosion model KD93 of
392 Kriebel and Dean²⁴. KD93 is based on the equilibrium profile concept and estimates shoreline retreat
393 and volumetric sand loss due to extreme waves and storm surge. KD93 input can be classified in (i)
394 hydrodynamic variables: significant wave height (H_s), peak wave period (T_p), wave incidence angle (α_w),
395 storm surge (η_s), tidal level (η_{tide}) and event duration; and (ii) parameters related to the beach profile:
396 dune height D , berm height B and width W , and the beach-face slope $\tan\theta_f$.

397 Storm surges for the present and future climate conditions are simulated using the DFLOW FM
398 model^{60,61} forced with the same 6-member CMIP5 Global Climate Model (GCM) ensemble as the wave
399 projections²⁰ (described in the previous section).

400 The hydrodynamic conditions driving episodic beach erosion are obtained from the wave and storm
401 surge projections. For each of the 6 GCMs we extracted the storm events simulated during the period

402 1980-2100, considering the parameters: max H_s , η_s , η_{tide} and T_p , as well as mean wave direction Dir_w , and
403 event duration. The extraction of storm events is based on the following criteria: (i) maximum H_s or η_s
404 exceeding the 90th percentile value; (ii) maximum T_p above 3 s; and (iii) maximum H_s above 0.5 m.

405 The offshore wave conditions are transformed to the nearshore(50 m depth) through wave refraction,
406 shoaling and breaking calculations based on Snell's law, following the approach described in Part II,
407 Chapter 2 of the US Army Corps Coastal engineering Manual⁶². The wave incidence angle required for
408 the calculations is obtained by combining the wave direction of each event from the model output with
409 the mean shoreline orientation. The active beach slope is obtained from the global dataset mentioned
410 above²³.

411 Subsequently, we simulate storm induced erosion for all the above events using KD93 on equilibrium
412 profiles, obtaining a sequence of shoreline retreat events for each transect. Subsequently, we apply
413 non-stationary extreme value statistical analysis⁶³ and fit a generalized Pareto distribution to the retreat
414 event series in order to obtain shoreline retreat estimates for different return periods. The present
415 analysis focuses on the storm-induced shoreline retreat for the 100-year retreat event S_{100} , and its
416 difference (ΔS_{100}) compared to present day conditions.

417 As storm retreat is estimated in a probabilistic manner through Monte Carlo simulations, the resulting
418 PDFs express the uncertainty from the wave projections (i.e. GCM ensemble spread and ocean model
419 error).

420 1.5 Spatial analysis

421 The study focusses on sandy beaches along the global coastline, which have been detected in a recent
422 study by discretizing the coast at 500 m alongshore transects¹. We use the Global Human Settlement
423 Layer⁶⁴ to estimate the population in low-lying coastal areas (i.e. elevation <10 m MSL) within a distance
424 of 25 km from each sandy beach transect. This serves as a proxy for the number of people benefiting
425 from nearby sandy beaches; either receiving natural protection from coastal storms, or benefiting from
426 beach amenity value, or other socio-economic activities related to tourism, beach-use, etc.

427 In order to identify regional patterns in shoreline dynamics, the global coastline is divided in 26
428 geographical regions (Extended Data Fig. 1), as defined in the IPCC Special Report on Managing the Risks
429 of Extreme Events and Disasters to Advance Climate Change Adaptation⁶⁵. The values discussed in the
430 manuscript correspond to averages for each region and country, or for the entire global coastline.

431 1.6 Statistical analysis

432 Equations 1 and 2 are applied here in a probabilistic manner, with the assumption that shoreline change
433 components R , S and AC are independent. PDFs of the three components are combined through Monte
434 Carlo simulations following the steps below²⁰: (i) random sampling from the individual PDFs; (ii) linear
435 addition of the dx_{shore} components according to equations 1 and 2; (iii) control of convergence to ensure
436 that the number of realizations is sufficient; (iv) joint PDF estimation. Typically one million realizations
437 are sufficient to obtain stable PDFs and convergence of the final percentiles. The resulting PDF of dx_{shore}
438 expresses the joint contributions from all components and the uncertainty therein (uncertainty factors
439 considered for each component are discussed in the final paragraph of the different dedicated sections
440 1.2-1.4).

441 We express the relative contribution of a component by the fraction of its median value to the median
442 total retreat. Similarly, relative contributions to the total dx_{shore} uncertainty is expressed by the fraction
443 of each component's variance to the total variance. We also estimate the difference between the
444 median dx_{shore} values for RCP4.5 and RCP8.5.

445 1.7 Limitations

446 The spatial and temporal scale of the analysis presented here imposes inevitable limitations related to
447 computational resources, data availability and methodological abstraction, the most important of which
448 are discussed below.

449 Ambient shoreline trends can be an important component of shoreline dynamics and depend on several
450 factors including the various sediment sources and sinks⁵⁷, along with the fate of sediments⁶⁶⁻⁶⁸. While
451 smaller-scale assessments considered in detail the above factors⁶⁹, limitations in terms of modelling
452 capabilities and available datasets, render application of such a methodology at global scale as
453 impossible. Therefore, in the present analysis we extrapolate historically observed ambient shoreline
454 changes AC into the future, as is common in previous studies^{58,70,71}. This is done, however, in a
455 probabilistic way that allows quantifying the temporal variability and inherent uncertainty. As such,
456 future ambient shoreline dynamics follow ongoing trends within uncertainty bounds defined by the
457 spread of the observed historical changes. The 32 year time window considered may be long enough to
458 express decadal-scale variability in shoreline position, but still may not fully resolve some rare cases of
459 coastline change, like those induced by very extreme events, or sudden and drastic human

460 interventions. Finally, the 30 m spatial resolution of the satellite dataset may not suffice to resolve
461 smaller displacements in less energetic areas.

462 Shoreline retreat due to SLR is estimated using the Bruun rule¹⁸, which despite its known drawbacks is
463 expected to be adequate for large scale assessments^{9,72}. The Bruun rule is based on the concept that the
464 morphology tends to reach an equilibrium state, which is supported by field observations^{40,73,74}.
465 However, the parameterization of the equilibrium profile *per se* has been a subject of debate⁷⁵⁻⁷⁷, as the
466 simplified model excludes several factors controlling coastal morphology often found in nature. These
467 include, for example, sediment sinks and sources⁶⁹, morphological response to SLR⁵⁹, morphological
468 control from natural or artificial structures⁶, the presence of nearshore bars⁷⁸ or other morphological
469 features^{79,80} and longshore processes⁶⁶.

470 Still, despite the criticism⁷⁵, the concept is being used extensively because any proposed improvements
471 and modifications^{53,81-85} demand data that are often not available. In the present implementation
472 several of the shortcomings of the Bruun rule are bypassed since *R* focusses only on what the concept
473 can deliver; i.e. alongshore-averaged shoreline response to SLR and changes in wave climate. Most of
474 the factors discussed above and that are beyond the Bruun rule's capacity are expressed by the ambient
475 change AC: e.g. changes due to sediment budget imbalances, geological or anthropogenic factors.

476 The uncertainty related to the active profile slope is another common weakness of the Bruun rule⁴¹,
477 which in the present analysis is addressed through the use of estimates obtained from topo-bathymetric
478 data. The quantitative accuracy of Bruun rule estimates has also been the subject of rigorous debate for
479 over 3 decades^{41,72,75,86}. Here we have attempted to address this source of uncertainty by incorporating a
480 correction factor *E* (Eq 5; see also discussion in Section 1.3), which is implemented probabilistically
481 within the Monte Carlo framework adopted in our computations.

482 Beach profile responses to storms are simulated using the KD93 model, rather than with sophisticated
483 process-based models that incorporate elaborate numerical methods and sediment transport
484 modules⁸⁷⁻⁹³. Such models can potentially provide more accurate estimations of storm erosion (if they
485 are well calibrated and validated), but require as input detailed topo-bathymetric and sediment grain
486 size information that is not available at global scale. The present analysis of *S* required the simulation of
487 circa 45 million storm events, rendering the application of models that are computationally more
488 expensive than KD93 practically impossible. In addition, KD93 has produced acceptable results in
489 previous smaller-scale applications of similar scope⁹⁴⁻⁹⁶.

490 An aspect not covered in our analysis is the effect of storm clusters. It has been discussed extensively in
491 previous studies, based either on field data^{40,42}, or numerical models^{87,97-99}, that storm chronology can
492 enhance the impact of individual events. These studies have also shown that storm erosion can be
493 followed by beach recovery. The latter is a complex process that is difficult to simulate^{73,100} and requires
494 in situ data. Predicting the maximum erosion from storm clusters at global scale is therefore a
495 challenging task. We consider only the episodic erosion from individual storms without accounting for
496 storm groups and do not simulate post-storm recovery. Rather it is assumed that the combined, long-
497 term, residual effects of erosion and recovery are included in the ambient change component AC.

498 The present analysis assumes unlimited backshore space for shoreline retreat. Some natural coastal
499 systems may have such accommodation space, while in other sites this may be strongly limited by
500 human development or physical barriers. This is a known issue which combined with SLR can have
501 societal and ecological implications discussed in the literature, especially under the term of coastal
502 squeeze^{101,102}. In principle, satellite imagery could provide formation on beach width¹⁰³ and available
503 space for coastal retreat at the backshore, yet such global dataset is not available. Socio-economic
504 projections suggest that coastal development will most likely continue in the decades to come^{12,13},
505 which may further reduce the accommodating space for coastal retreat. We consider arbitrary erosion
506 threshold values to indicate potential changes that could be critical for sandy beaches. With the
507 information on backshore space and development that may be available at local/regional scales, our
508 publicly available projections could be used by scientists and practitioners to carry out more detailed
509 smaller-scale assessments.

510 1.8 Additional Results

511 Sea level rise retreat

512 Rising sea levels will result in shoreline retreat along the entire global coastline with the exception of a
513 few regions that experience uplift, like the Baltic Sea (Extended Data Fig. 2). The global average median
514 R by 2050 (relative to 2010) is projected to be around -28 m and -35 m under RCP4.5 and RCP8.5,
515 respectively. By the end of the century, SLR-driven erosion is projected to further grow to around -63 m
516 and -105 m, respectively. The retreat of sandy beaches due to SLR is projected to be highest (at least 130
517 m by 2100 relative to 2010 under RCP8.5) in North Australia, Central North America, North-East Brazil,
518 South and Southeast Asia, and Central Europe. Other regions for which high R values are projected
519 include West Africa, Southeastern South America, South Australia/New Zealand, East Asia and East
520 North America.

521 **Ambient changes**

522 The present section discusses long-term ambient changes as a result of hydrodynamic, geological and
523 anthropic factors. The global averaged *AC* is erosive, corresponding to global average land retreat of -
524 11.5 m by 2050 (very likely range between -34.7 and 11.7 m) and of -30.4 m by the end of the century
525 (very likely range between -79.1 and 18.2 m). The stronger erosion is projected for South Asia, the
526 Caribbean SIDS, and Southeastern South America with the very likely range by the end of the century
527 being from -431.8 to -238.2, from -250 to -174.2, and from -204.5 to -71.3, respectively (Extended Data
528 Fig. 3). East Asia shows a strong accretive ambient shoreline change trend (very likely range: 86.7-147.6),
529 being the result of major coastal land reclamations over the recent decades.

530 Smaller scale projections show high spatial variability with erosive and accretive trends interchanging.
531 Examples of accretion hotspots in Central America/Mexico can be found in Colombia, both on the
532 Caribbean Sea and on the Pacific Ocean, especially at the mouths of the rivers Atrato, Sinu, Magdalena,
533 Jurubida, San Juan and others. In Central North America, the long-term trends of coastal
534 erosion/accretion are dominated by the dynamics at the mouth of the Mississippi river. The area is very
535 dynamic, with large erosive spots (e.g. the Terrebonne Bay) and accretive spots (e.g. the Atchafalaya
536 delta¹⁰⁴). Furthermore, the area is frequently hit by tropical cyclones¹⁰⁵ that may cause abrupt extreme
537 erosion, for example hurricane Katrina, the largest natural disaster in the history of the US¹⁰⁶, and
538 hurricane Rita in 2005.

539 In North-Eastern Brazil, the activity is dominated by the morpho-dynamics of the Tocantins delta and
540 along the coasts of Para-Maranhao-Piaui-Ceara, a very active area characterized by both extreme
541 coastal erosion and accretion⁷. The dominance of accretion is likely due to the erosivity of the soil in the
542 interior, a rich river network that transports sediments towards the sea, and strong macro-tidal currents
543 carrying them along the coasts¹⁰⁷.

544 The most active areas in Southern Africa are the coasts of Mozambique and the Western coasts of
545 Madagascar, areas characterized by intense tidal currents. Accretion prevails especially in Madagascar,
546 likely due to internal erosion and subsequent transport of sediment towards the coasts, and
547 redistribution of it by currents¹⁰⁸.

548 Southeast Asia is characterized by both extreme erosion and accretion. Intense erosion can be observed,
549 for example, at the deltas of the rivers Sittaung¹⁰⁹ and Mekong¹⁹, or in areas of strong land subsidence,
550 like the Northern coast of Java¹¹⁰, or in the northern Manila Bay¹¹¹. Examples of areas dominated by
551 extreme accretion are the extended delta of the Red river in North Vietnam, western New Guinea,

552 several river deltas in the Malaysian peninsula and Sumatra, as well as in intensely built sites such as
553 Bangkok and Singapore. A more detailed discussion on the local/regional variations can be found in
554 Mentaschi et al.⁷.

555 Acknowledgments

556 RR is supported by the AXA Research fund and the Deltares Strategic Research Programme 'Coastal and
557 Offshore Engineering'. PA is supported by the EU Horizon 2020 Programme for Research and Innovation,
558 under grant agreement no. 776613 (EUCP: EUropean Climate Prediction system).

559 Author contributions

560 M.I.V, R.R. and L.F. jointly conceived the study. M.I.V. and L.M. produced the storm surge and wave
561 projections. L.M. produced the ambient shoreline change data. M.I.V. and T.A.P. produced the storm
562 erosion and sea level rise retreat projections, P.A. produced the global beach slope dataset, A.L.
563 produced the global sandy beach presence dataset. M.I.V. analysed the data and prepared the
564 manuscript, with all authors discussing results and implications and commenting on the manuscript at
565 all stages. T.P. was funded by the research group RNM-328 of the Andalusian Research Plan (PAI) and
566 the Portuguese Science and Technology Foundation (FCT) through the grant UID/MAR/00350/2013
567 attributed to CIMA of the University of Algarve. The corresponding author would like to thank Drs
568 Alessio Giardino and Ap van Dongeren for providing helpful comments on the manuscript and the
569 methodology.

570 **Competing interests:** the Authors declare no Competing Financial or Non-Financial Interest

571 Data availability

572 The models and datasets presented are part of the integrated risk assessment tool LISCoAsT (Large scale
573 Integrated Sea-level and Coastal Assessment Tool) developed by the Joint Research Centre of the
574 European Commission. The dataset is available through the LISCoAsT repository of the JRC data
575 collection (<http://data.europa.eu/89h/18eb5f19-b916-454f-b2f5-88881931587e>) and should be cited as
576 follows:

577 European Commission, Joint Research Centre (2019): Global shoreline change projections.

578 European Commission, Joint Research Centre (JRC) [Dataset] doi:10.2905/18EB5F19-B916-454F-B2F5-
579 88881931587E; PID: <http://data.europa.eu/89h/18eb5f19-b916-454f-b2f5-88881931587e>

580 [Code availability](#)

581 The code that supported the findings of this study is available from the corresponding author upon
582 reasonable request.

583 [Methods References](#)

- 584 33 Meinshausen, M. *et al.* The RCP greenhouse gas concentrations and their extensions from 1765
585 to 2300. *Clim. Change* **109**, 213-241, doi:10.1007/s10584-011-0156-z (2011).
- 586 34 Hurst, M. D., Rood, D. H., Ellis, M. A., Anderson, R. S. & Dornbusch, U. Recent acceleration in
587 coastal cliff retreat rates on the south coast of Great Britain. *Proceedings of the National
588 Academy of Sciences* **113**, 13336-13341, doi:10.1073/pnas.1613044113 (2016).
- 589 35 Ruggiero, P. Is the Intensifying Wave Climate of the U.S. Pacific Northwest Increasing Flooding
590 and Erosion Risk Faster Than Sea-Level Rise? *Journal of Waterway, Port, Coastal, and Ocean
591 Engineering* **139**, 88-97, doi:doi:10.1061/(ASCE)WW.1943-5460.0000172 (2013).
- 592 36 Loureiro, C., Ferreira, Ó. & Cooper, J. A. G. Extreme erosion on high-energy embayed beaches:
593 Influence of megarips and storm grouping. *Geomorphology* **139–140**, 155-171,
594 doi:<http://dx.doi.org/10.1016/j.geomorph.2011.10.013> (2012).
- 595 37 Kroon, A. *et al.* Statistical analysis of coastal morphological data sets over seasonal to decadal
596 time scales. *Coastal Eng.* **55**, 581-600 (2008).
- 597 38 Gallop, S. L., Bosserelle, C., Pattiaratchi, C. & Eliot, I. Rock topography causes spatial variation in
598 the wave, current and beach response to sea breeze activity. *Mar. Geol.* **290**, 29-40,
599 doi:10.1016/j.margeo.2011.10.002 (2011).
- 600 39 Voudoukis, M. I., Velegrakis, A. F. & Plomaritis, T. A. Beachrock occurrence, characteristics,
601 formation mechanisms and impacts. *Earth-Science Reviews* **85**, 23-46,
602 doi:10.1016/j.earscirev.2007.07.002 (2007).
- 603 40 Voudoukis, M. I., Almeida, L. P. & Ferreira, Ó. Beach erosion and recovery during consecutive
604 storms at a steep-sloping, meso-tidal beach. *Earth Surf. Processes Landforms* **37**, 583-691,
605 doi:10.1002/esp.2264 (2012).
- 606 41 Ranasinghe, R., Callaghan, D. & Stive, M. J. F. Estimating coastal recession due to sea level rise:
607 beyond the Bruun rule. *Clim. Change* **110**, 561-574, doi:10.1007/s10584-011-0107-8 (2012).
- 608 42 Coco, G. *et al.* Beach response to a sequence of extreme storms. *Geomorphology* **204**, 493-501,
609 doi:<http://dx.doi.org/10.1016/j.geomorph.2013.08.028> (2014).
- 610 43 Hardisty, J. in *Sediment Transport and Depositional Processes* (ed K. Pye)216-255 (Blackwell,
611 1994).
- 612 44 Pekel, J.-F., Cottam, A., Gorelick, N. & Belward, A. S. High-resolution mapping of global surface
613 water and its long-term changes. *Nature* **540**, 418, doi:10.1038/nature20584

614 <https://www.nature.com/articles/nature20584#supplementary-information> (2016).
- 615 45 Haklay, M. & Weber, P. OpenStreetMap: User-Generated Street Maps. *IEEE Pervasive
616 Computing* **7**, 12-18, doi:10.1109/MPRV.2008.80 (2008).
- 617 46 Boak, E. H. & Turner, I. L. Shoreline Definition and Detection: A Review. *J. Coast. Res.*, 688-703,
618 doi:doi:10.2112/03-0071.1 (2005).
- 619 47 Jackson, L. P. & Jevrejeva, S. A probabilistic approach to 21st century regional sea-level
620 projections using RCP and High-end scenarios. *Global Planet. Change* **146**, 179-189,
621 doi:<http://dx.doi.org/10.1016/j.gloplacha.2016.10.006> (2016).
- 622 48 Yamazaki, D. *et al.* A high-accuracy map of global terrain elevations. *Geophys. Res. Lett.* **44**,
623 5844-5853, doi:doi:10.1002/2017GL072874 (2017).

- 624 49 Weatherall, P. *et al.* A new digital bathymetric model of the world's oceans. *Earth and Space*
625 *Science* **2**, 331-345, doi:doi:10.1002/2015EA000107 (2015).
- 626 50 Hallermeier, R. J. in *16th International Conference on Coastal Engineering*.1493-1512 (ASCE).
- 627 51 Nicholls, R. J., Birkemeier, W. A. & Lee, G.-h. Evaluation of depth of closure using data from
628 Duck, NC, USA. *Mar. Geol.* **148**, 179-201 (1998).
- 629 52 Baron, H. M. *et al.* Incorporating climate change and morphological uncertainty into coastal
630 change hazard assessments. *Nat. Hazards* **75**, 2081-2102, doi:10.1007/s11069-014-1417-8
631 (2015).
- 632 53 Ranasinghe, R., Duong, T. M., Uhlenbrook, S., Roelvink, D. & Stive, M. Climate-change impact
633 assessment for inlet-interrupted coastlines. *Nature Climate Change* **3**, 83,
634 doi:10.1038/nclimate1664
- 635 <https://www.nature.com/articles/nclimate1664#supplementary-information> (2012).
- 636 54 Voudoukas, M. I., Mentaschi, L., Voukouvalas, E., Verlaan, M. & Feyen, L. Extreme sea levels on
637 the rise along Europe's coasts. *Earth's Future*, n/a-n/a, doi:10.1002/2016EF000505 (2017).
- 638 55 Queffeulou, P. & Croizé-Fillon, D. Global altimeter SWH data set. (*Laboratoire d'Océanographie
639 Spatiale, IFREMER*, 2014).
- 640 56 Li, F. *Probabilistic estimation of dune erosion and coastal zone risk* PhD Thesis thesis, Delft
641 University of Technolog, (2014).
- 642 57 Toimil, A., Losada, I. J., Camus, P. & Díaz-Simal, P. Managing coastal erosion under climate
643 change at the regional scale. *Coastal Eng.* **128**, 106-122,
644 doi:<https://doi.org/10.1016/j.coastaleng.2017.08.004> (2017).
- 645 58 Le Cozannet, G. *et al.* Quantifying uncertainties of sandy shoreline change projections as sea
646 level rises. *Scientific Reports* **9**, 42, doi:10.1038/s41598-018-37017-4 (2019).
- 647 59 Lentz, E. E. *et al.* Evaluation of dynamic coastal response to sea-level rise modifies inundation
648 likelihood. *Nature Clim. Change* **6**, 696–700, doi:10.1038/nclimate2957
- 649 <http://www.nature.com/nclimate/journal/vaop/ncurrent/abs/nclimate2957.html#supplementary-information> (2016).
- 650 60 Jagers, B. R., J. L.; Verlaan, M.; Lalic, A.; Genseberger, M.; Friocourt, Y.; van der Pijl, S. in
651 *American Geophysical Union, Fall Meeting 2014*(San Francesco, USA, 2014).
- 652 61 Muis, S., Verlaan, M., Winsemius, H. C., Aerts, J. C. J. H. & Ward, P. J. A global reanalysis of storm
653 surges and extreme sea levels. *Nat Commun* **7**, doi:10.1038/ncomms11969 (2016).
- 654 62 US Army Corps of Engineers. *Coastal Engineering Manual*. (U.S. Army Corps of Engineers, 2002).
- 655 63 Mentaschi, L. *et al.* Non-stationary Extreme Value Analysis: a simplified approach for Earth
656 science applications. *Hydrol. Earth Syst. Sci. Discuss.* **2016**, 1-38, doi:10.5194/hess-2016-65
657 (2016).
- 658 64 Corbane, C. *et al.* Big earth data analytics on Sentinel-1 and Landsat imagery in support to global
659 human settlements mapping. *Big Earth Data* **1**, 118-144, doi:10.1080/20964471.2017.1397899
660 (2017).
- 661 65 IPCC. *Managing the Risks of Extreme Events and Disasters to Advance Climate Change
662 Adaptation. A Special Report of Working Groups I and II of the Intergovernmental Panel on
663 Climate Change*. (Cambridge University Press, 2012).
- 664 66 Antolínez, J. A. A. *et al.* A multiscale climate emulator for long-term morphodynamics (MUSCLE-
665 morpho). *Journal of Geophysical Research: Oceans* **121**, 775-791, doi:doi:10.1002/2015JC011107
666 (2016).
- 667 67 Enríquez, A. R., Marcos, M., Álvarez-Ellacuría, A., Orfila, A. & Gomis, D. Changes in beach
668 shoreline due to sea level rise and waves under climate change scenarios: application to the
669

- 670 Balearic Islands (western Mediterranean). *Nat. Hazards Earth Syst. Sci.* **17**, 1075-1089,
671 doi:10.5194/nhess-17-1075-2017 (2017).
- 672 68 Anderson, D., Ruggiero, P., Antolínez, J. A. A., Méndez, F. J. & Allan, J. A Climate Index Optimized
673 for Longshore Sediment Transport Reveals Interannual and Multidecadal Littoral Cell Rotations.
674 *Journal of Geophysical Research: Earth Surface* **123**, 1958-1981, doi:10.1029/2018JF004689
675 (2018).
- 676 69 Giardino, A. *et al.* A quantitative assessment of human interventions and climate change on the
677 West African sediment budget. *Ocean Coast. Manag.* **156**, 249-265,
678 doi:<https://doi.org/10.1016/j.occecoaman.2017.11.008> (2018).
- 679 70 Vitousek, S., Barnard, P. L., Limber, P., Erikson, L. & Cole, B. A model integrating longshore and
680 cross-shore processes for predicting long-term shoreline response to climate change. *Journal of*
681 *Geophysical Research: Earth Surface* **122**, 782-806, doi:10.1002/2016jf004065 (2017).
- 682 71 Wainwright, D. J. *et al.* Moving from deterministic towards probabilistic coastal hazard and risk
683 assessment: Development of a modelling framework and application to Narrabeen Beach, New
684 South Wales, Australia. *Coastal Eng.* **96**, 92-99,
685 doi:<https://doi.org/10.1016/j.coastaleng.2014.11.009> (2015).
- 686 72 Ranasinghe, R. & Stive, M. J. F. Rising seas and retreating coastlines. *Clim. Change* **97**, 465,
687 doi:10.1007/s10584-009-9593-3 (2009).
- 688 73 Davidson, M. A., Splinter, K. D. & Turner, I. L. A simple equilibrium model for predicting shoreline
689 change. *Coastal Eng.* **73**, 191-202, doi:<http://dx.doi.org/10.1016/j.coastaleng.2012.11.002>
690 (2013).
- 691 74 Ozkan-Haller, T., Brundidge, S. Equilibrium Beach Profiles for Delaware Beaches. 147-160 (2007).
- 692 75 Cooper, J. A. G. & Pilkey, O. H. Sea-level rise and shoreline retreat: time to abandon the Bruun
693 Rule. *Global Planet. Change* **43**, 157-171, doi:<http://dx.doi.org/10.1016/j.gloplacha.2004.07.001>
694 (2004).
- 695 76 Pilkey, O. H. & Dixon, K. L. *The Corps and the Shore.*(Island Press, 1996).
- 696 77 Pilkey, O. H. *et al.* The Concept of Shoreface Profile of Equilibrium: A Critical Review. *Journal of*
697 *Coastal Research SI* **9**, 225-278 (1993).
- 698 78 Holman, R. A., Lalejini, D. M., Edwards, K. & Veeramony, J. A parametric model for barred
699 equilibrium beach profiles. *Coastal Eng.* **90**, 85-94,
700 doi:<http://dx.doi.org/10.1016/j.coastaleng.2014.03.005> (2014).
- 701 79 Coco, G. & Murray, A. B. Patterns in the sand: From forcing templates to self-organization.
702 *Geomorphology* **91**, 271-290, doi:10.1016/j.geomorph.2007.04.023 (2007).
- 703 80 Voudoukas, M. I. Erosion/accretion and multiple beach cusp systems on a meso-tidal, steeply-
704 sloping beach. *Geomorphology* **141-142**, 34-46, doi:doi:10.1016/j.geomorph.2011.12.003
705 (2012).
- 706 81 Wang, Z. & Dean, R. G. in *Coastal Sediments '07* 626-632 (American Society of Civil Engineers,
707 2007).
- 708 82 Dai, Z.-J., Du, J.-z., Li, C.-C. & Chen, Z.-S. The configuration of equilibrium beach profile in South
709 China. *Geomorphology* **86**, 441-454, doi:<http://dx.doi.org/10.1016/j.geomorph.2006.09.016>
710 (2007).
- 711 83 Romanczyk, W., Boczar-Karakiewicz, B. & Bona, J. L. Extended equilibrium beach profiles.
712 *Coastal Eng.* **52**, 727-744, doi:<https://doi.org/10.1016/j.coastaleng.2005.05.002> (2005).
- 713 84 Anderson, T. R., Fletcher, C. H., Barbee, M. M., Frazer, L. N. & Romine, B. M. Doubling of coastal
714 erosion under rising sea level by mid-century in Hawaii. *Nat. Hazards* **78**, 75-103,
715 doi:10.1007/s11069-015-1698-6 (2015).
- 716 85 Bray, M. & Hooke, J. Prediction of soft-cliff retreat with accelerating sea-level rise. *J. Coast. Res.*
717 **13**, 453-467 (1997).

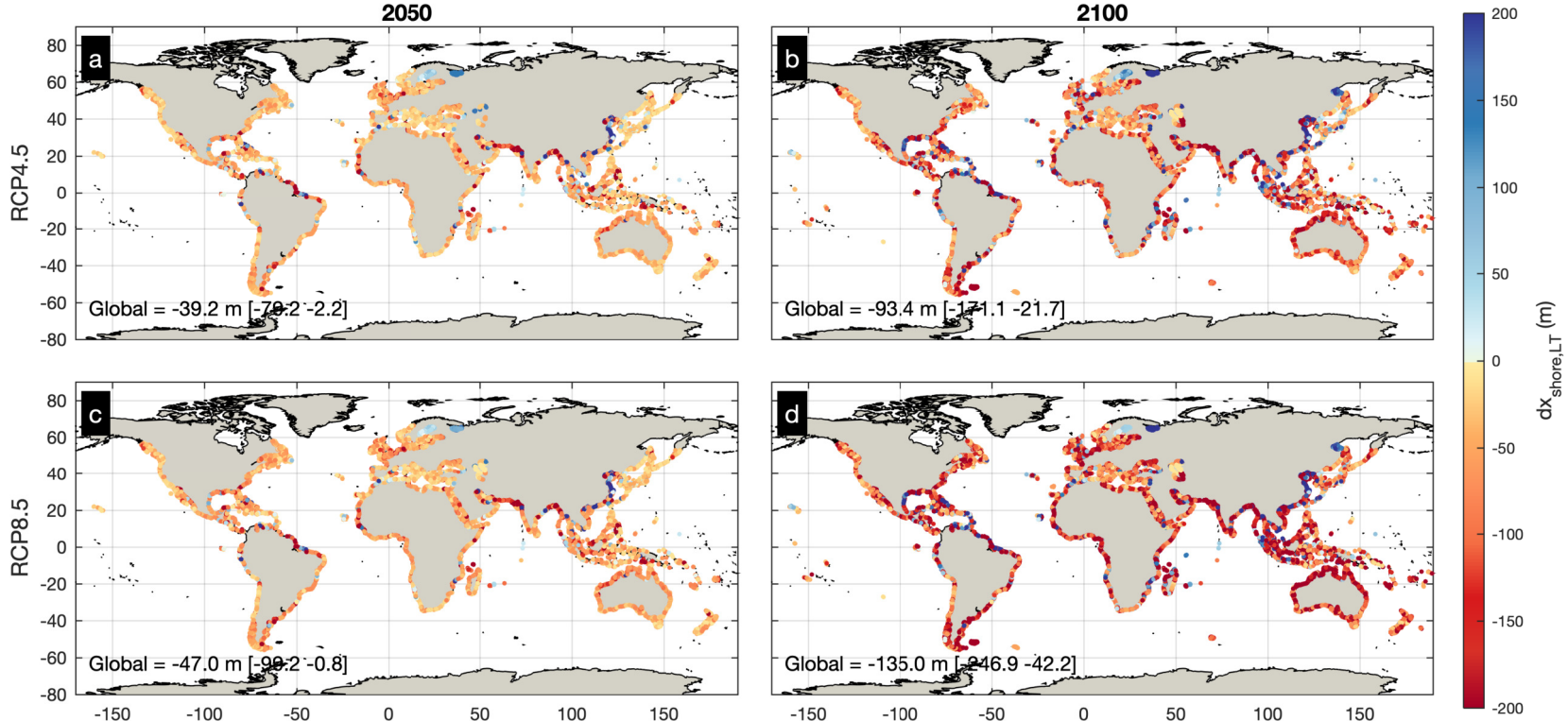
- 718 86 Pilkey, O. H. & Cooper, J. A. G. Society and Sea Level Rise. *Science* **303**, 1781,
719 doi:10.1126/science.1093515 (2004).
- 720 87 Splinter, K. D., Carley, J. T., Golshani, A. & Tomlinson, R. A relationship to describe the
721 cumulative impact of storm clusters on beach erosion. *Coastal Eng.* **83**, 49-55,
722 doi:<http://dx.doi.org/10.1016/j.coastaleng.2013.10.001> (2014).
- 723 88 Voudoukis, M. I., Ferreira, O., Almeida, L. P. & Pacheco, A. Toward reliable storm-hazard
724 forecasts: XBeach calibration and its potential application in an operational early-warning
725 system. *Ocean Dyn.* **62**, 1001-1015, doi:10.1007/s10236-012-0544-6 (2012).
- 726 89 Roelvink, D. *et al.* Modelling storm impacts on beaches, dunes and barrier islands. *Coastal Eng.*
727 **56**, 1133-1152 (2009).
- 728 90 Broekema, Y. B. *et al.* Observations and modelling of nearshore sediment sorting processes
729 along a barred beach profile. *Coastal Eng.* **118**, 50-62,
730 doi:<https://doi.org/10.1016/j.coastaleng.2016.08.009> (2016).
- 731 91 de Winter, R. C. & Ruessink, B. G. Sensitivity analysis of climate change impacts on dune erosion:
732 case study for the Dutch Holland coast. *Clim. Change* **141**, 685-701, doi:10.1007/s10584-017-
733 1922-3 (2017).
- 734 92 Karunaratna, H., Brown, J., Chatzirodou, A., Dissanayake, P. & Wisse, P. Multi-timescale
735 morphological modelling of a dune-fronted sandy beach. *Coastal Eng.* **136**, 161-171,
736 doi:<https://doi.org/10.1016/j.coastaleng.2018.03.005> (2018).
- 737 93 Passeri, D. L., Bilskie, M. V., Plant, N. G., Long, J. W. & Hagen, S. C. Dynamic modeling of barrier
738 island response to hurricane storm surge under future sea level rise. *Clim. Change* **149**, 413-425,
739 doi:10.1007/s10584-018-2245-8 (2018).
- 740 94 Callaghan, D. P., Nielsen, P., Short, A. D. & Ranasinghe, R. Statistical simulation of wave climate
741 and extreme beach erosion. *Coastal Eng.* **55**, 375-390 (2008).
- 742 95 Ferreira, Ó., Garcia, T., Matias, A., Taborda, R. & Dias, J. A. An integrated method for the
743 determination of set-back lines for coastal erosion hazards on sandy shores. *Cont. Shelf Res.* **26**,
744 1030-1044 (2006).
- 745 96 Mull, J. & Ruggiero, P. Estimating Storm-Induced Dune Erosion and Overtopping along U.S. West
746 Coast Beaches. *J. Coast. Res.*, 1173-1187, doi:10.2112/JCOASTRES-D-13-00178.1 (2014).
- 747 97 Ferreira, Ó. Storm groups versus extreme single storms: Predicted erosion and management
748 consequences. *Journal of Coastal Research* **42**, 155-161 (2005).
- 749 98 Dissanayake, P., Brown, J. & Karunaratna, H. Impacts of storm chronology on the
750 morphological changes of the Formby beach and dune system, UK. *Nat. Hazards Earth Syst. Sci.
751 Discuss.* **3**, 2565-2597, doi:10.5194/nhessd-3-2565-2015 (2015).
- 752 99 Hackney, C., Darby, S. E. & Leyland, J. Modelling the response of soft cliffs to climate change: A
753 statistical, process-response model using accumulated excess energy. *Geomorphology* **187**, 108-
754 121, doi:<https://doi.org/10.1016/j.geomorph.2013.01.005> (2013).
- 755 100 Yates, M. L., Guza, R. T. & O'Reilly, W. C. Equilibrium shoreline response: Observations and
756 modeling. *Journal of Geophysical Research C: Oceans* **114** (2009).
- 757 101 Pontee, N. Defining coastal squeeze: A discussion. *Ocean Coast. Manag.* **84**, 204-207,
758 doi:<https://doi.org/10.1016/j.occecoaman.2013.07.010> (2013).
- 759 102 Doody, J. P. Coastal squeeze and managed realignment in southeast England, does it tell us
760 anything about the future? *Ocean Coast. Manag.* **79**, 34-41,
761 doi:<https://doi.org/10.1016/j.occecoaman.2012.05.008> (2013).
- 762 103 Monioudi, I. N. *et al.* Assessment of island beach erosion due to sea level rise: the case of the
763 Aegean archipelago (Eastern Mediterranean). *Nat. Hazards Earth Syst. Sci.* **17**, 449-466,
764 doi:10.5194/nhess-17-449-2017 (2017).

- 765 104 Rosen, T. & Xu, Y. J. Recent decadal growth of the Atchafalaya River Delta complex: Effects of
766 variable riverine sediment input and vegetation succession. *Geomorphology* **194**, 108-120,
767 doi:<https://doi.org/10.1016/j.geomorph.2013.04.020> (2013).
- 768 105 Peduzzi, P. *et al.* Global trends in tropical cyclone risk. *Nature Clim. Change* **2**, 289-294,
769 doi:<http://www.nature.com/nclimate/journal/v2/n4/abs/nclimate1410.html#supplementary-information> (2012).
- 770 106 Travis, J. Scientists' Fears Come True as Hurricane Floods New Orleans. *Science* **309**, 1656,
771 doi:[10.1126/science.309.5741.1656](https://doi.org/10.1126/science.309.5741.1656) (2005).
- 772 107 Monteiro, M. C., Pereira, L. C. C. & de Oliveira, S. M. O. Morphodynamic Changes of a Macrotidal
773 Sand Beach in the Brazilian Amazon Coast (Ajuruteua-Pará). *J. Coast. Res.*, 103-107 (2009).
- 774 108 Salomon, J.-N. L'accréation littorale sur la côte Ouest de Madagascar. *Physio-Géo* **3**,
775 doi:[10.4000/physio-geo.671](https://doi.org/10.4000/physio-geo.671) (2009).
- 776 109 Taft, L. & Evers, M. A review of current and possible future human–water dynamics in
777 Myanmar's river basins. *Hydrol. Earth Syst. Sci.* **20**, 4913-4928, doi:[10.5194/hess-20-4913-2016](https://doi.org/10.5194/hess-20-4913-2016)
778 (2016).
- 780 110 Marfai, M. A. & King, L. Monitoring land subsidence in Semarang, Indonesia. *Environ. Geol.* **53**,
781 651-659, doi:[10.1007/s00254-007-0680-3](https://doi.org/10.1007/s00254-007-0680-3) (2007).
- 782 111 Rodolfo, K. S. & Siringan, F. P. Global sea-level rise is recognised, but flooding from
783 anthropogenic land subsidence is ignored around northern Manila Bay, Philippines. *Disasters* **30**,
784 118-139, doi:[10.1111/j.1467-9523.2006.00310.x](https://doi.org/10.1111/j.1467-9523.2006.00310.x) (2006).

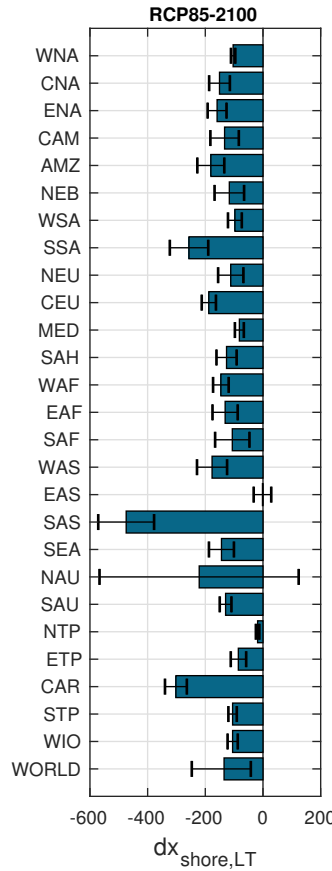
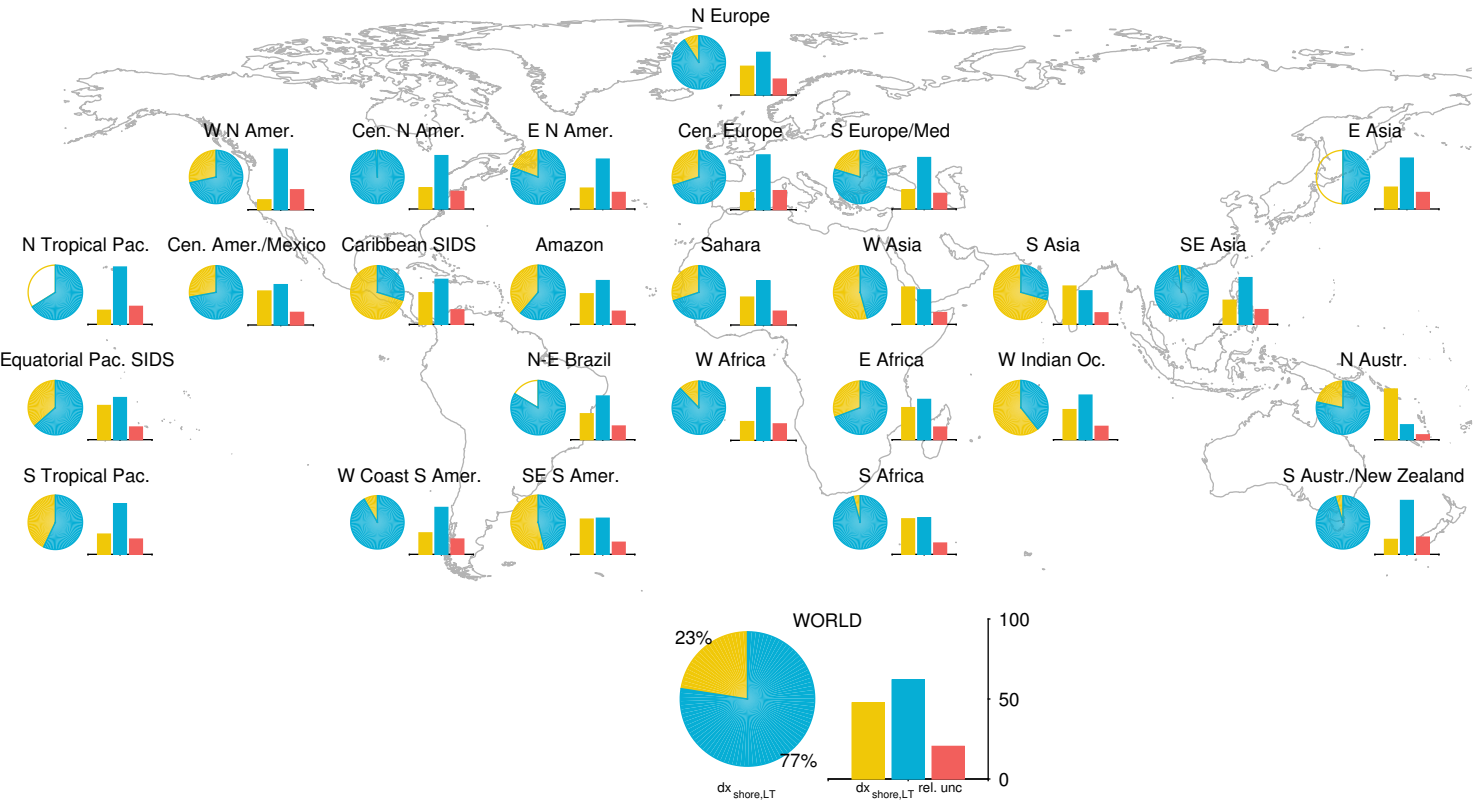
785

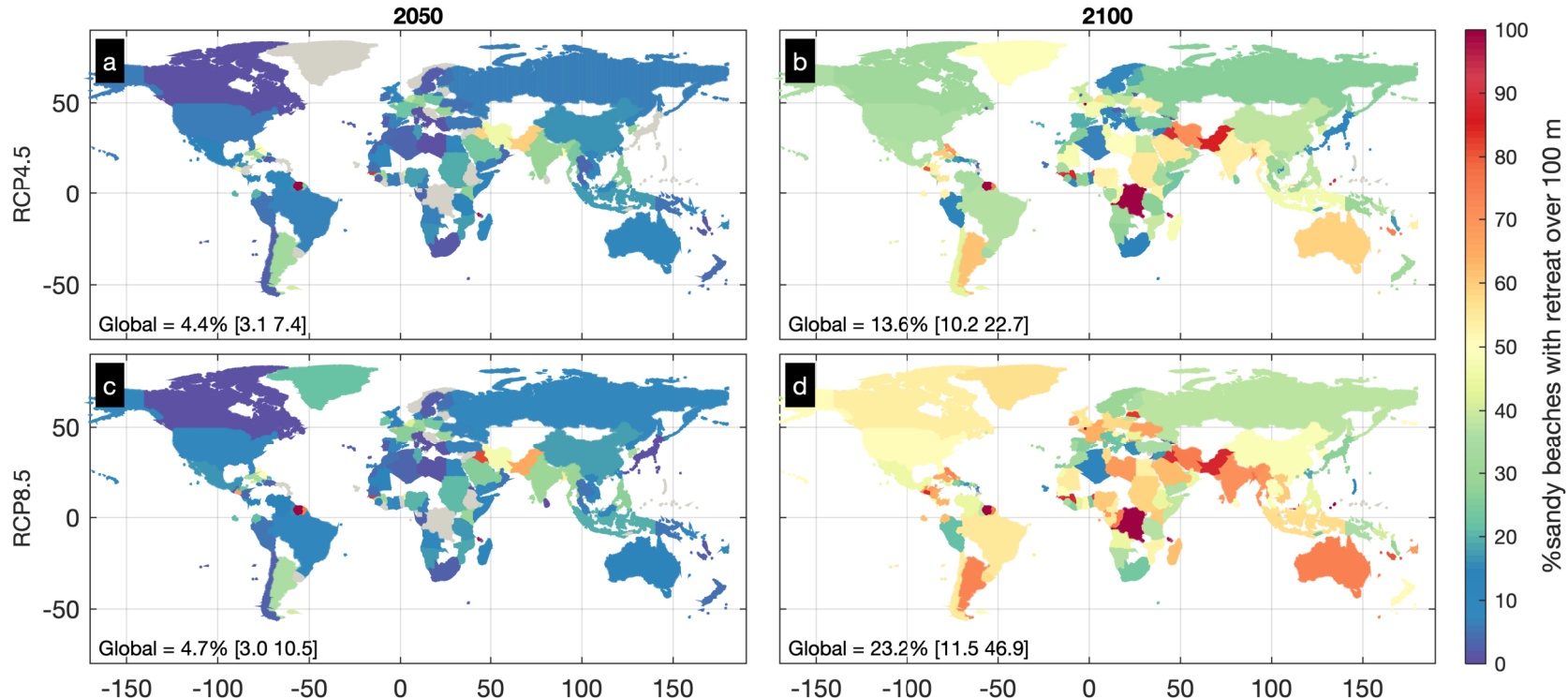
786

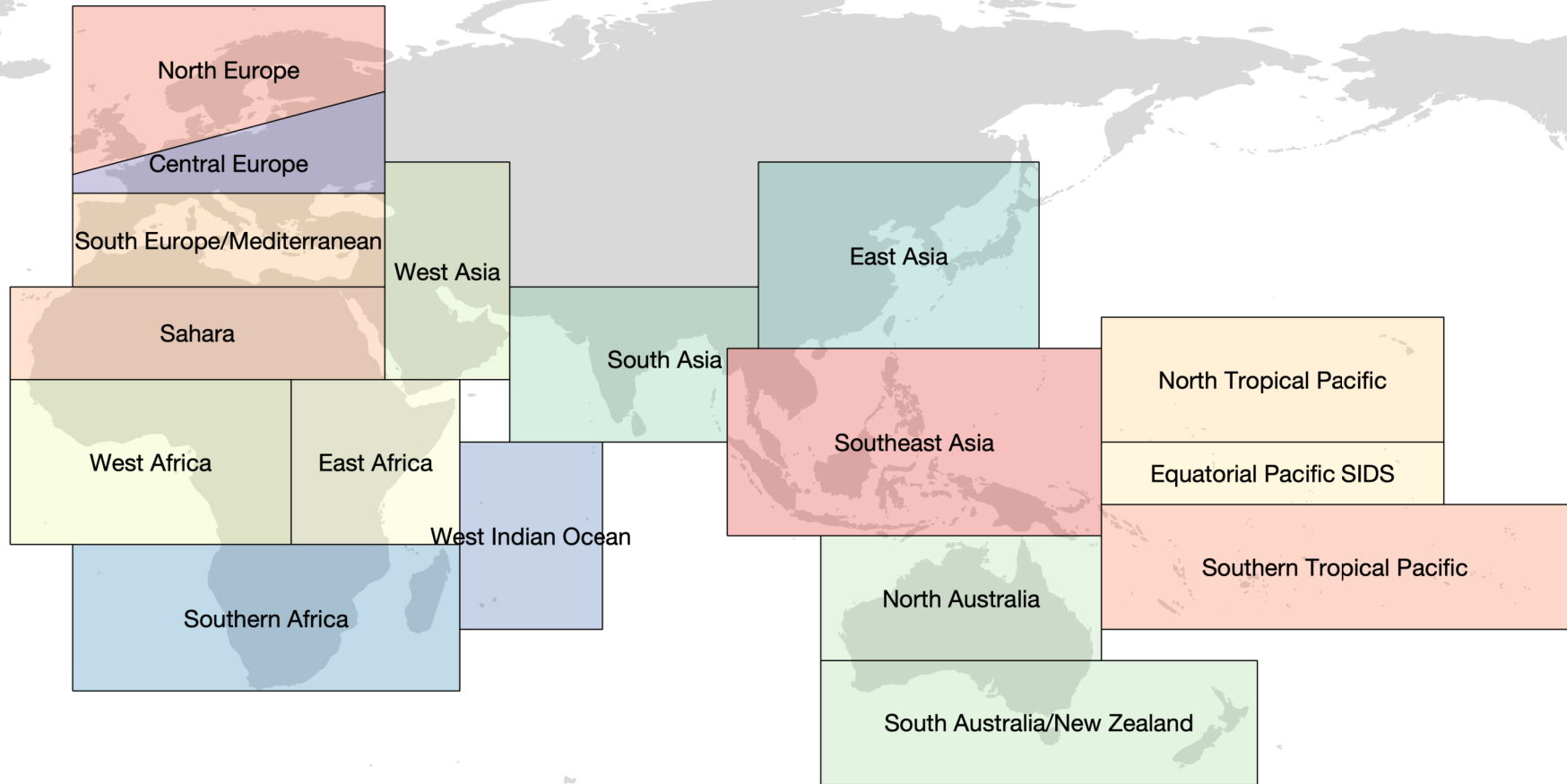
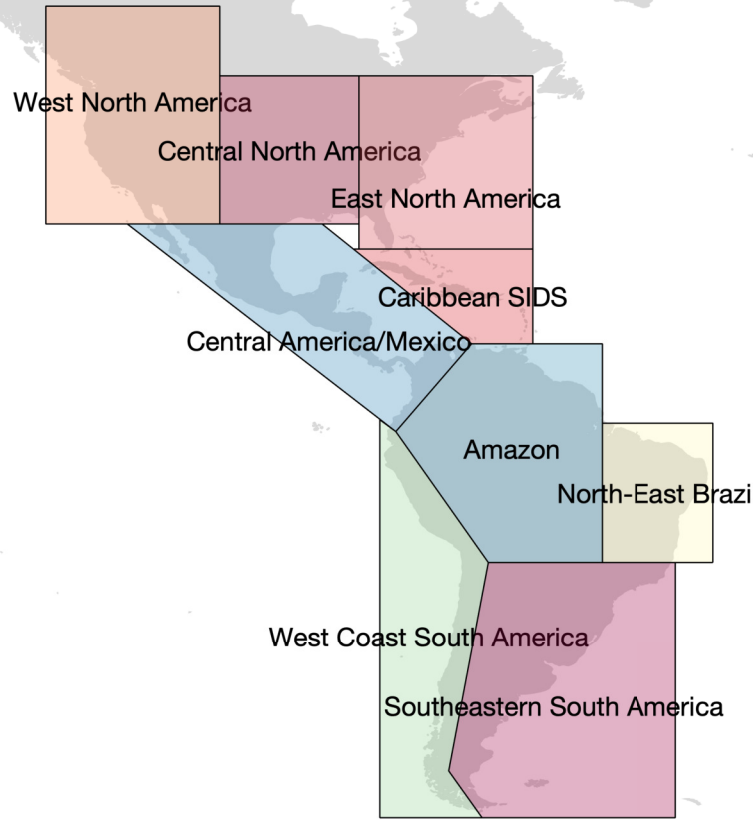
787

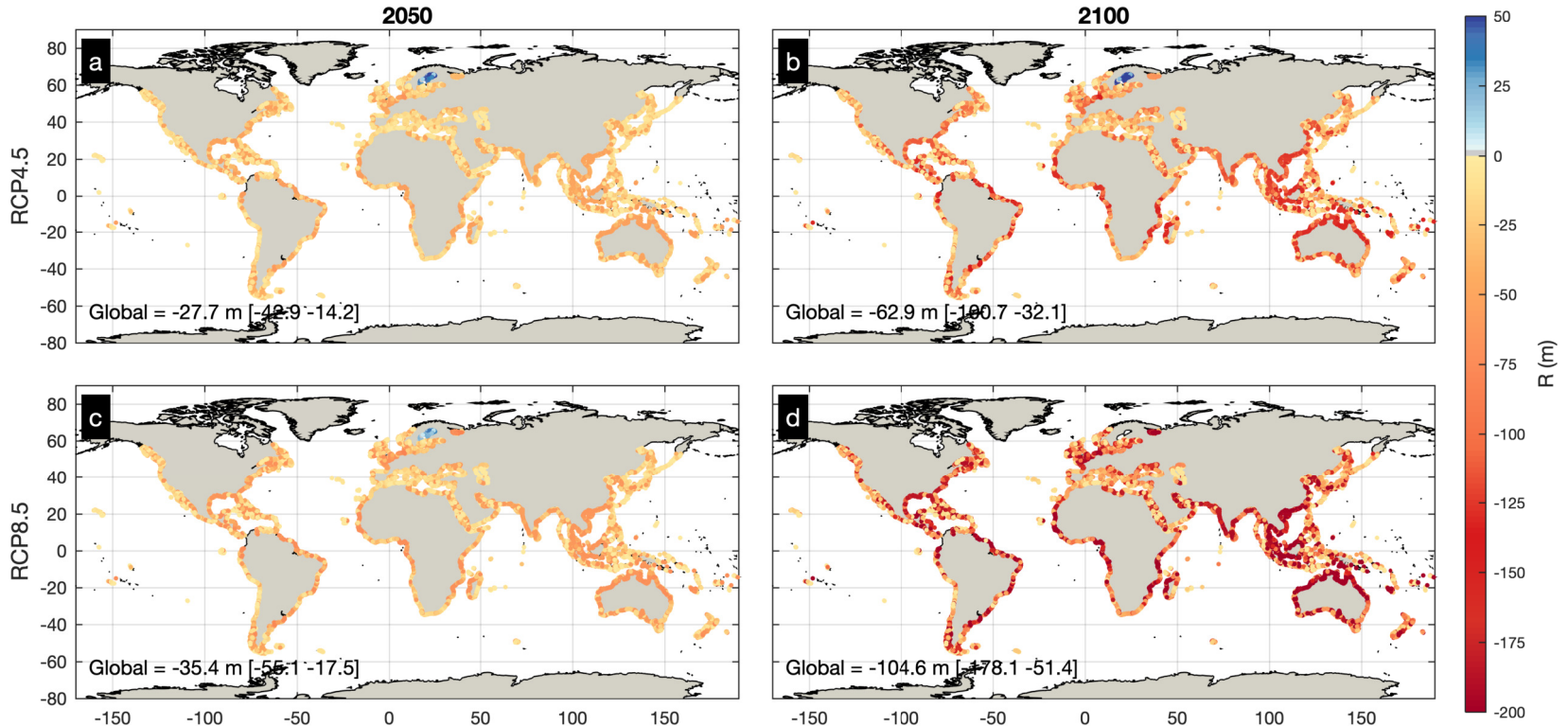


Ambient Change SLR Retreat RCP Shoreline Change

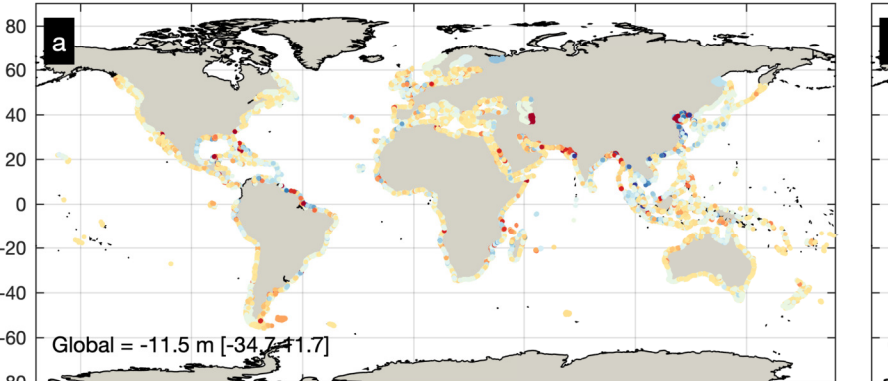




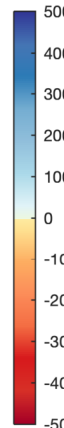
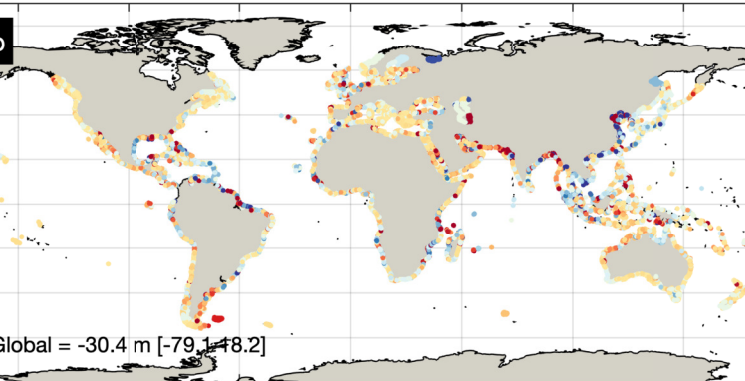


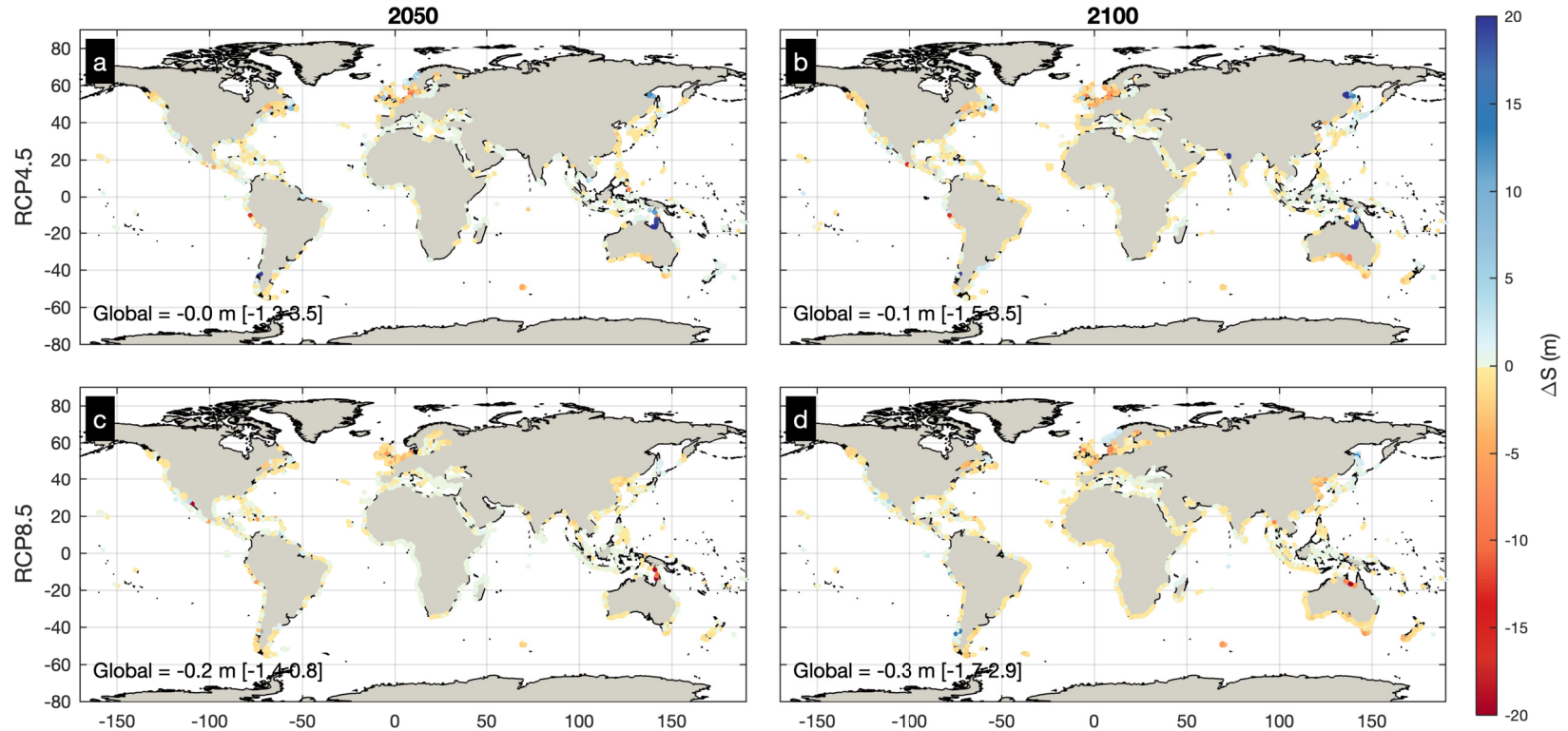


2050



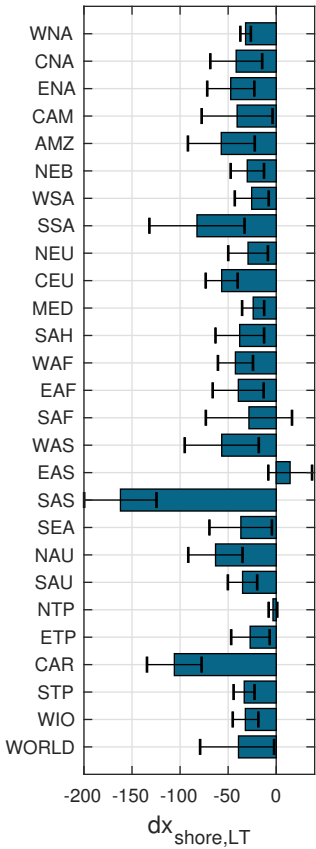
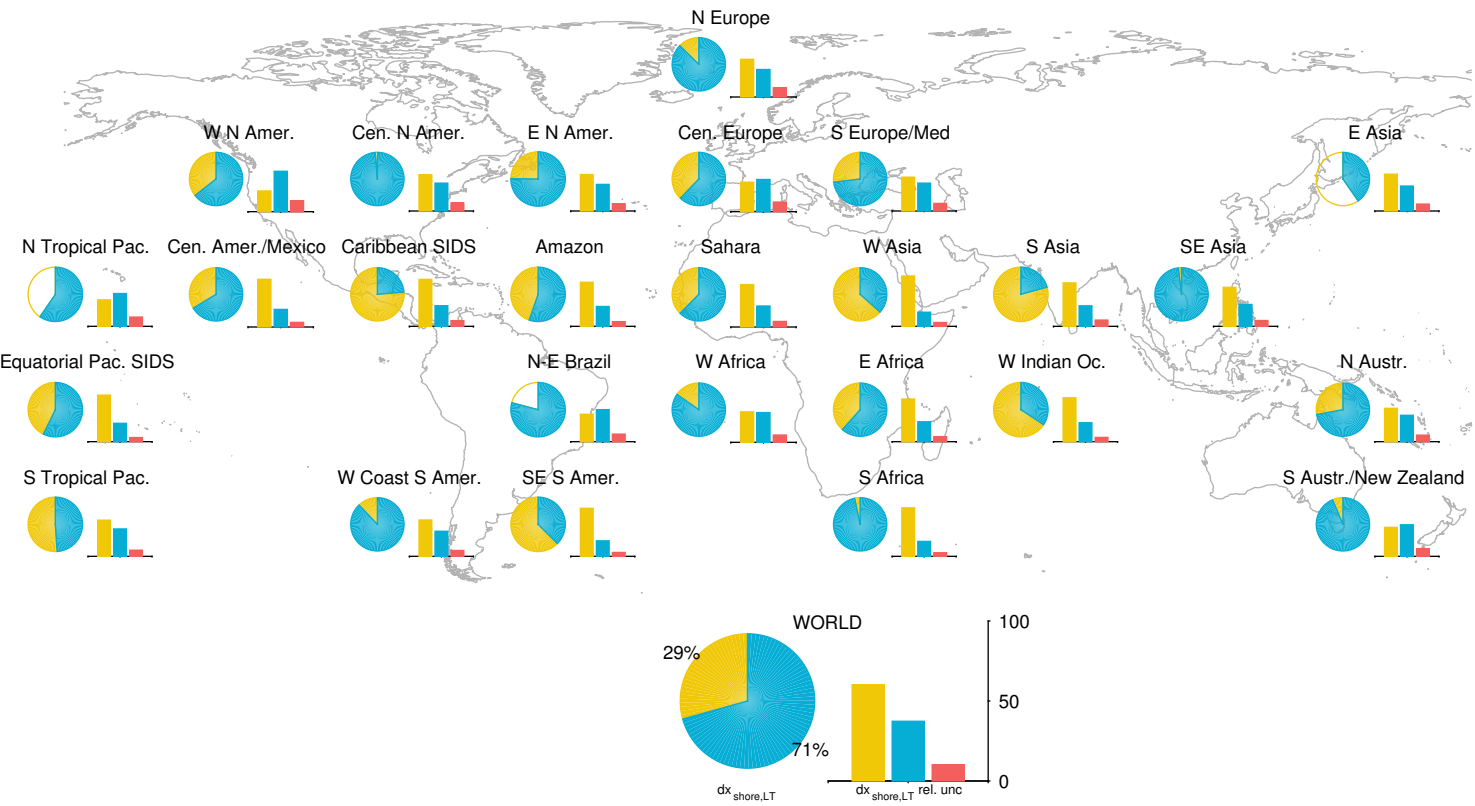
2100





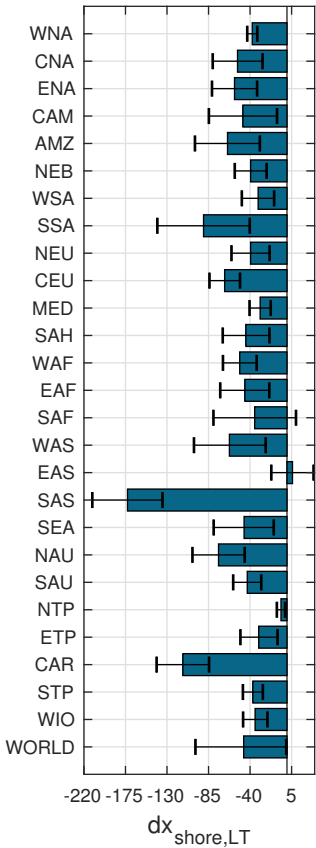
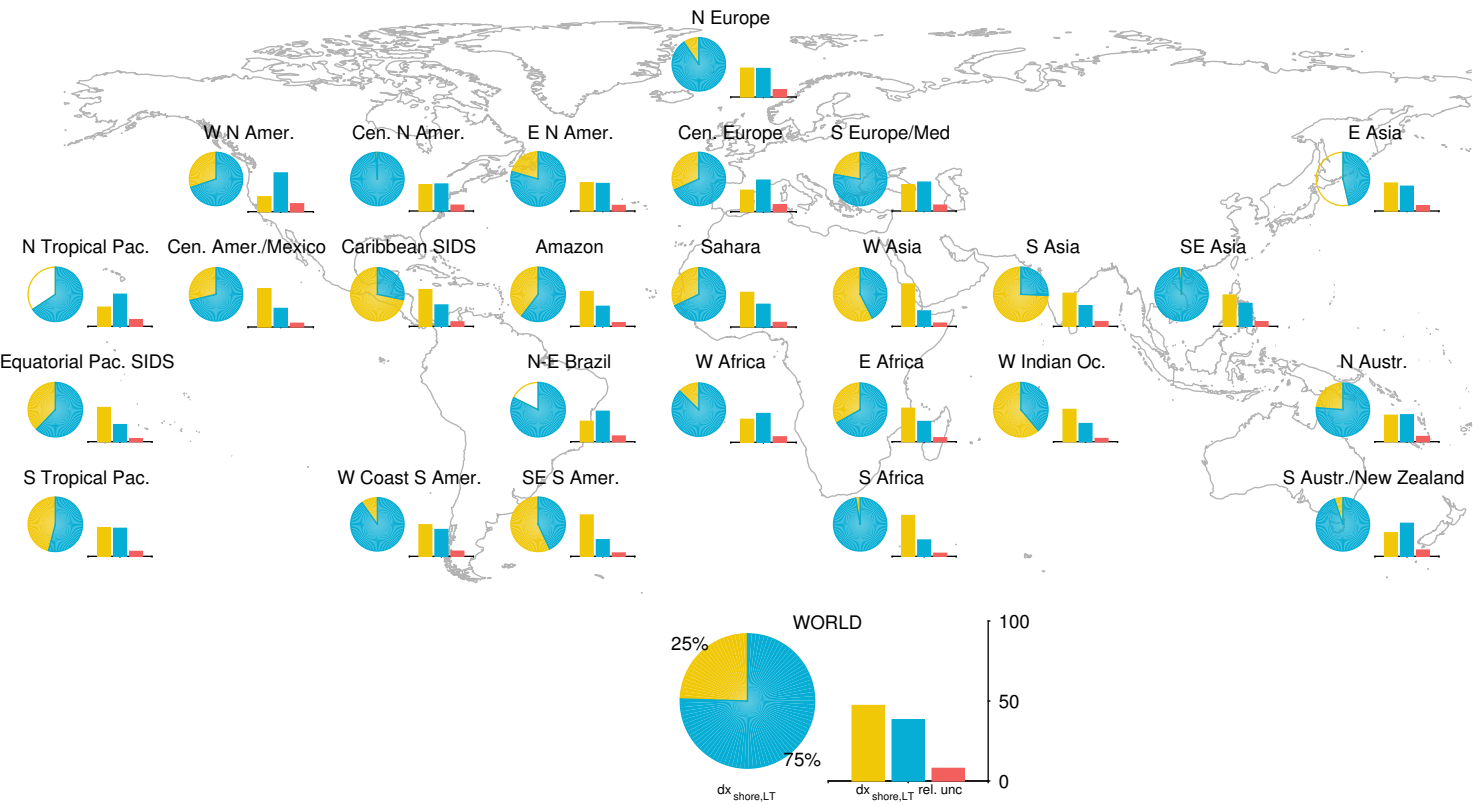
Ambient Change SLR Retreat RCP Shoreline Change

RCP45-2050

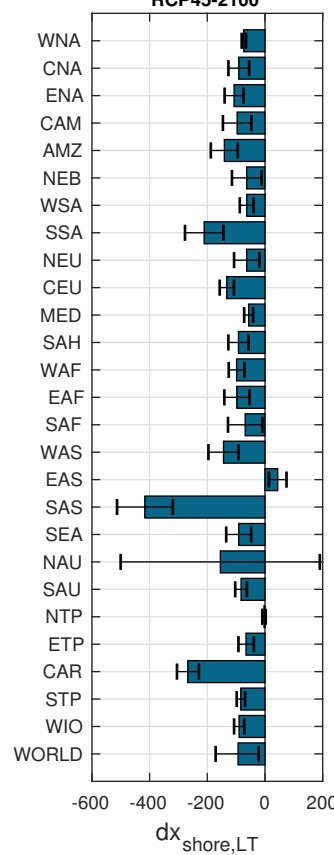
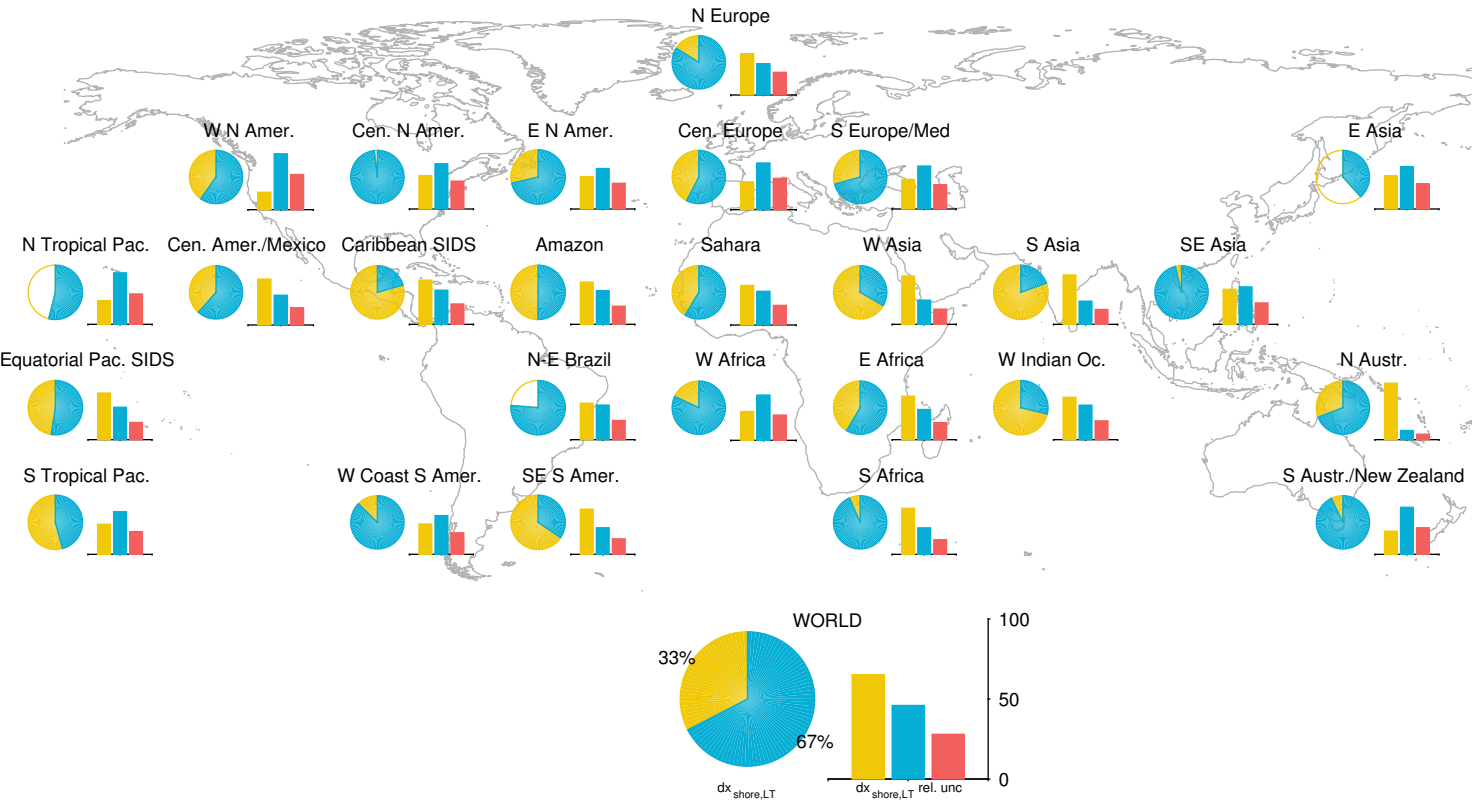


Ambient Change SLR Retreat RCP Shoreline Change

RCP85-2050



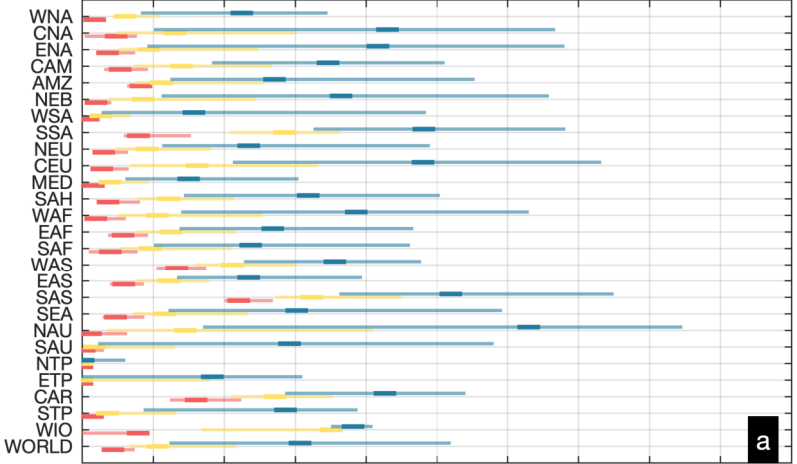
Ambient Change SLR Retreat RCP Shoreline Change



RCP4.5

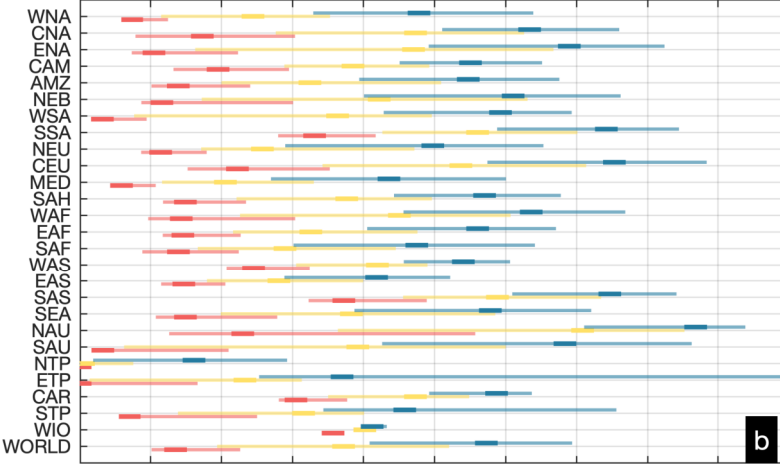


2050



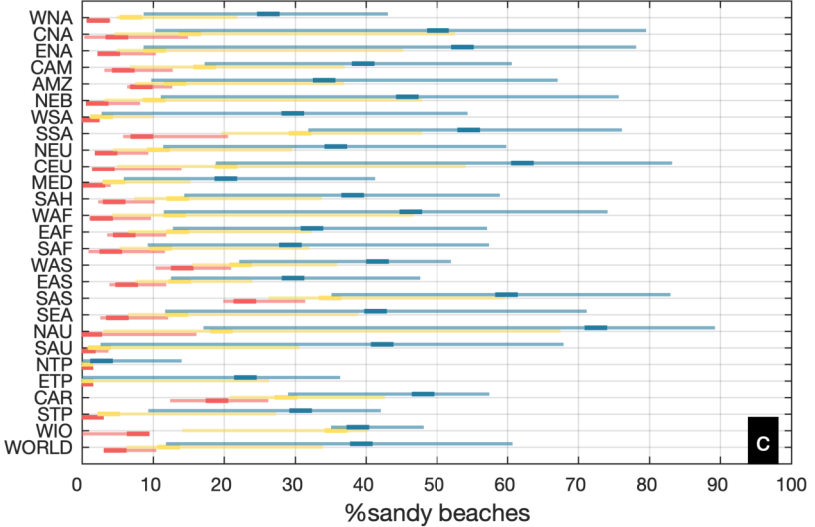
a

2100

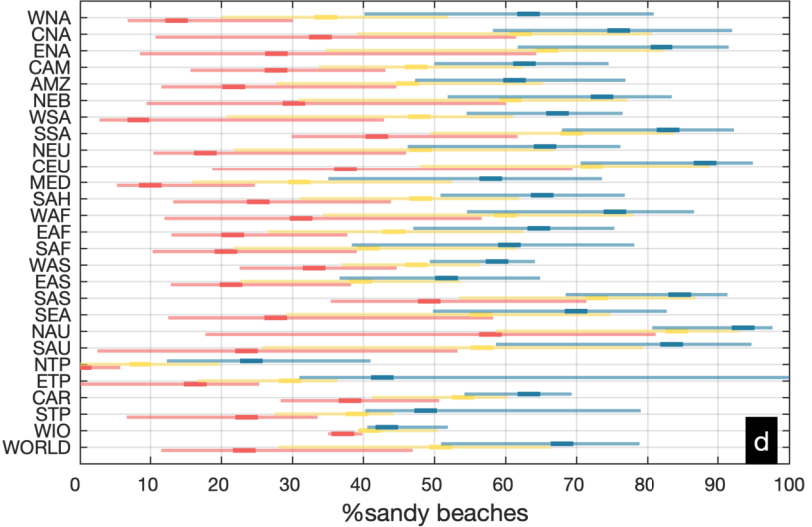


b

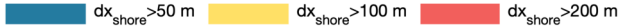
RCP8.5



c

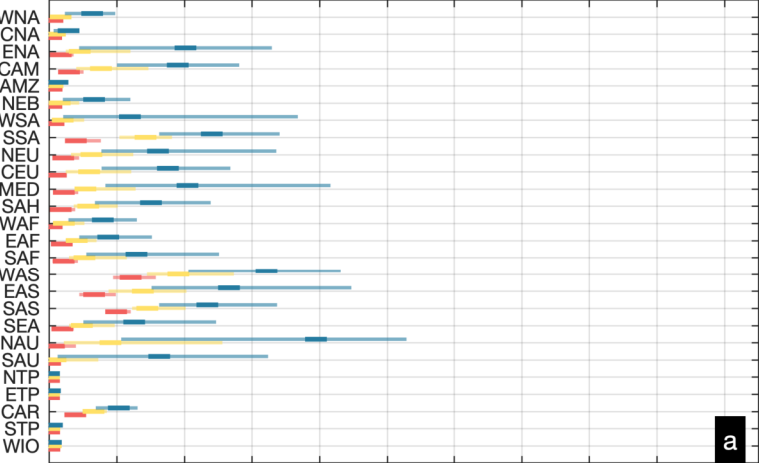


d



2050

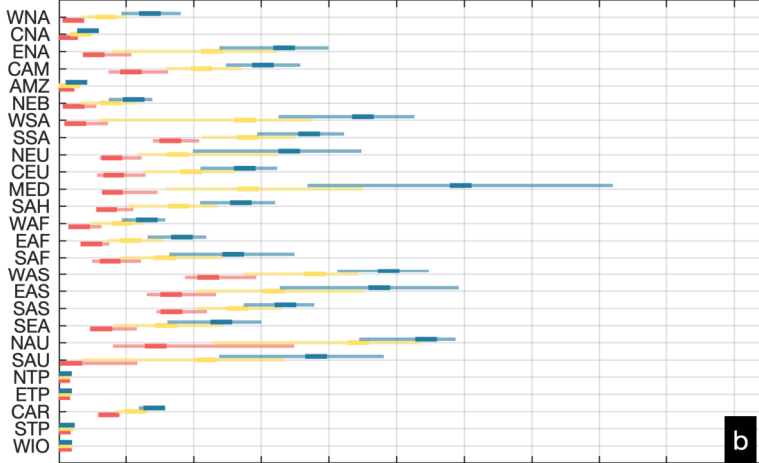
RCP4.5



a

2100

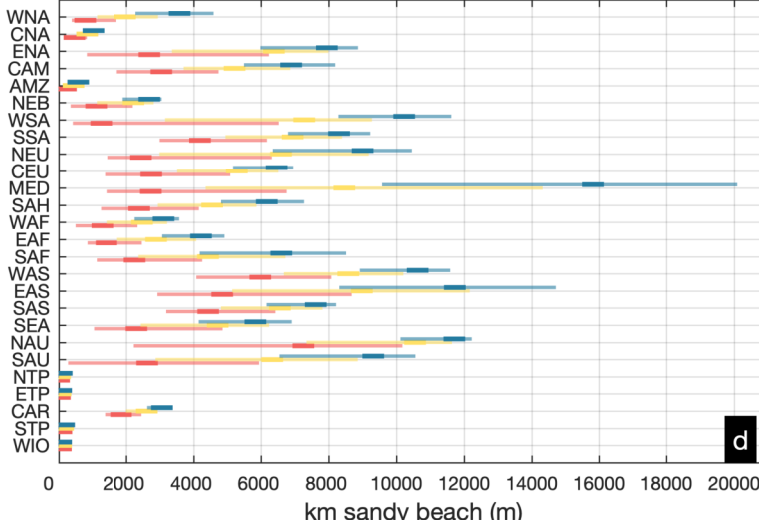
RCP8.5



b

km sandy beach (m)

c



d

km sandy beach (m)

